Assimilation of satellite data by 4D-VAR at ECMWF

Jean-Noël Thépaut

European Centre for Medium-range Weather Forecasts, Reading, UK.

Abstract

A variational analysis scheme has been developed at ECMWF within the framework of the Integrated Forecasting System (IFS). The scheme can be run in its three-dimensional (3D-VAR) or four-dimensional (4D-VAR) version.

Technically speaking, 3D-VAR can be seen as a 0 time-step 4D-VAR assimilation. Scientifically speaking, the main crucial difference between 4D-VAR and 3D-VAR is the ability of the former to implicitly specify flow-dependent structure functions.

4D-VAR seeks a model solution which is as close as possible, in a least-square sense, to the observations available over a given time period (and to any other available information). The model trajectory is constrained to fit these observations by adjusting its initial conditions. The information extracted from the observations is then consistent with the dynamics of the model. Moreover, 4D-VAR allows the use of the observations at the appropriate time, which is of particular interest for asynoptic observations such as satellite data.

After describing the theory and the practical implementation of 4D-VAR at ECMWF, we present on "one single observation" experiments the impact we can expect from 4D over 3D-VAR. Along the same lines, the multivariate nature of 4D-VAR implied through the time dimension is described with a 1D advection model.

The potential of 4D-VAR is then illustrated with real assimilations using different sorts of asynoptic satellite data: namely scatterometer sigma-noughts, TOVS cleared radiances and SSMI precipitable water content (PWC) observations.

1 Introduction.

One of the motivations to develop a variational analysis scheme (see Pailleux et al., 1991) is that it circumvents some of the practical OI weaknesses, since it allows the analysis to use all the observations at every model grid point, and can easily handle a non trivial link between the model state and such observations like satellite data. In its four-dimensional formulation (4D-VAR), the method consistently uses the information coming from the observations and the dynamics of the model.

Over a limited period of time, it is expected to produce a similar result as what produced from the full extended Kalman filter approach (see Thépaut and Courtier, 1991 and Daley, 1991) and at a much lower cost.

1.1 The 4D-VAR problem.

A four-dimensional (4d) variational assimilation (4D-VAR) seeks an optimal balance between observations scattered in time and space over a finite 4d analysis volume and *a priori* information (Thépaut and Courtier, 1991; Rabier and Courtier, 1992; Thépaut et al., 1993a). The key *a priori* information used in 4D-VAR is knowledge of the dynamics of the atmosphere. In addition 4D-VAR ordinarily uses an estimate of the initial conditions, i.e., the atmospheric state at the start of the analysis period, and an estimate of the error statistics of the initial conditions.

The principle of 4D-VAR is then to find a model solution which is as close as possible, in a least-square sense, to the observations available over a time period $[t_0, t_n]$. (The reader is referred to Lorenc (1986) for a full presentation of the material of this section). The misfit to the data and other approximate constraints is measured by a cost function. The smaller the cost function, the better the fit. For the case of Gaussian errors, a squared error cost function of the form given below should be used (Lorenc, 1986). In the present case an approximate constraint is based on a background, x_b, which is an *a priori* estimate of x_0, the model state at the initial time t_0. (We will use the term background to refer generally to an *a priori* estimate and specifically to x_b, as well as to forecasts made from x_b within the analysis period $[t_0, t_n]$.) If there are exact constraints, these are used to reduce the dimension of the control variable. In the present case the model dynamics are an exact constraint and the control variable is thereby reduced to x_0. These considerations lead to defining $J(x_0)$, the cost function for 4D-VAR by,

$$J(x_0) = \frac{1}{2}(H(x_0) - y)^T O^{-1}(H(x_0) - y) + \frac{1}{2}(x_0 - x_b)^T B^{-1}(x_0 - x_b) \qquad (1)$$

Here y is the vector of observations distributed in time and space, H is the operator which predicts the observations from the model initial state, O is the covariance matrix of the observation and representativeness errors and B is the covariance matrix of the errors of x_b. In practice in the IFS system (Pailleux et al., 1991) the first term on the right hand side of (1) is broken up into a sum of smaller terms for different times and different observing systems by assuming the errors at different times and for different observing systems are uncorrelated, i.e. by assuming O is block diagonal. First, the data are binned

into one hour time intervals. Then all data in each bin are assumed to be observed at the central time of the bin. Second the different data sources are divided. Finally, geographic divisions of the data within a bin for a single data source are made as necessary.

Note that (1) is also the cost function for 3D-VAR if x_0 is replaced by x, the model state at the synoptic analysis time. For 3D-VAR H provides the interpolation to the observation locations and the calculation of the observed variables. In 4D-VAR H also includes the action of the forecast model.

1.2 The equivalence of 4D-VAR and the Kalman filter.

It has been often stated that under certain conditions the solution of the 4D-VAR problem and that of the Kalman-Bucy filter are identical (e.g. Daley, 1991). Both methods and the arguments showing this equivalence are outlined by Lorenc (1986). As noted by Daley (1991, page 384) this equivalence is exact over a given time period $[t_0, t_n]$ only when

- The forecast model is linear.
- The interpolation operator H is linear.
- The forecast model is perfect.
- The forecast error covariance for the Kalman filter at time t_0 is equal to the background error covariance B used in 4D-VAR.

Also the equivalence holds only for the analyses produced at t_n. That is, for any time within the analysis time period the 4D-VAR solution is influenced by data throughout the time period, whereas the Kalman filter analyses at any particular time makes use only of previous data. The 4D-VAR solution, under the above conditions, is exactly equivalent to the fixed interval Kalman smoother over the interval $[t_0, t_n]$. The interested reader is referred to Jazwinski (1970), who derives the Kalman smoother from the same maximum likelihood principle which leads to the 4D-VAR minimization problem.

A consequence of the theoretical equivalence between the two methods is the implicit use in 4D-VAR of flow-dependent forecast error covariances. In general one expects that the application of a full Kalman filter to a 4D data assimilation problem will lead to inhomogeneous forecast error covariances since these covariances are the initial background error covariances evolved according to the linearized model dynamics. The exact transport in time of the forecast error covariance matrix is not tractable with the actual resolution of the operational models. The practical advantage of 4D-VAR comes about because the forecast error covariances are not explicitly computed. However, they are implicitly used in the 4D-VAR assimilation. The single observation experiments reported here allow us to visualize the forecast error covariances of the Kalman filter equivalent to the 4D-VAR.

The equivalence of 4D-VAR and the Kalman filter is only approximate: The forecast model is not linear, but over the 24 hour period the evolution of perturbations is approximately linear, see e.g. Lacarra and Talagrand (1988) (the 4D-VAR solutions would be little effected if the tangent linear model were used in place of the nonlinear model). The interpolation operator is in fact very close to linear. Here we consider only the case when

the observation is of a model variable at a grid point. Finally, the forecast model is far from perfect, but we limit our comparison to a Kalman filter which ignores model errors.

First we note that for an optimal analysis x_a, such as from 3D-VAR, or an idealized OI or from the analysis performed at each step of the Kalman filter, the analysis increments, $x_a - x_b$, are a linear combination of the observation increments, $y - H(x_b)$, (Lorenc, 1986, equation 28),

$$x_a - x_b = BH'^T(H'BH'^T + O)^{-1}[y - H(x_b)] \tag{2}$$

where the matrix H' is the linearization of H in the vicinity of the current state x_b. For the Kalman filter x_b is the forecast from the previous analysis and B and H are defined accordingly. In the case of a single observation, located at a model grid point, and taking the model state to be a grid point representation, H'^T becomes a vector as long as the model state vector contains all zeros except for a single one corresponding to the observation variable and location. In this special case (2) simplifies to

$$x_a - x_b = \left(\frac{y - x_{b\alpha}}{b_{\alpha\alpha} + o_{\alpha\alpha}}\right) B_\alpha \tag{3}$$

where α indexes the observation in the model state vector so that $b_{\alpha\alpha}$ is the background covariance of the observation variable and location, $o_{\alpha\alpha}$ is the observation variance and B_α is the column of B corresponding to the observation variable and location. This shows that the analysis increments are proportional to B_α, i.e. to the covariance of the background error at the observation variable and location with the background error of all other model variables and locations. Note that (3) shows that at the observation location, the analysis increment is smaller in magnitude than the observation increment. However depending on the structure of $b_\alpha\alpha$ the analysis increments at other locations can be larger than the observation increment.

This relationship also holds for the 4D-VAR solutions at t_n in our single observation experiments because the 4D-VAR solution at t_n is equivalent to the corresponding Kalman filter solution for this problem. The corresponding Kalman filter is one in which there are no model errors and no other observations. In such a case the only actions of the Kalman filter until the final analysis are to advance the model state and the error covariances of the model state to t_n. Thus the 4D-VAR solution for a single observation at t_n is a column of the predicted covariance matrix of the corresponding Kalman filter. This covariance matrix is predicted using linear dynamics, which simplifies in this case to

$$B(t_n) = RB(t_0)R^T \tag{4}$$

where R is the tangent linear model dynamics for the period $[t_0, t_n]$.

To date no one has applied the Kalman filter to an atmospheric model (nor to any other model) with 300000 degrees of freedom. However, thanks to the analysis presented here, the results of Section 2 demonstrate just how complex the predicted error covariances can become in such a case, in just 24 h. This very complexity has important implications for the eventual implementation of the Kalman filter—any approximations made in modeling the covariances must still be capable of representing very complex structures. It must be noted that the covariances calculated here are imperfect, suffering from the assumption of

a perfect model inherent in 4D-VAR, and the uncertainty in our estimates of the statistics of the observational and background errors.

An assessment of the 4D-VAR potential has been performed at ECMWF these last few years. The material presented in the next following sections has been described in detail in the following papers : Andersson et al. (1993), Thépaut et al. (1993b) and Filiberti (1993).

We will first describe in a "one single observation" experiment framework, the structure functions (section 2) implicitly used in 4D-VAR as compared to those usually specified in 3D-VAR.

In section 3, we will demonstrate on a very simple model the multivariate nature of 4D-VAR due to the time dimension involved in the assimilation, and in particular the ability of 4D-VAR to infer information on non directly observed fields.

We will then illustrate the potential of 4D-VAR on three sets of experiments where different types of satellite data have been used, showing that this new system is a good candidate for assimilating future asynoptic remote sensing data.

2 Single observation experiments.

As discussed in Section 1.2, 4D-VAR implicitly evolves the background covariances in time. Thus in contrast to simplified sequential assimilation schemes such as 3D-VAR, 4D-VAR is able to implicitly specify flow-dependent covariance functions. Here we study the case of the small intense storm which caused extensive damage in Brittany and southwestern England on 16 October 1987 (Jarraud et al., 1989). We find that within 4D-VAR, a single key datum, indicating the position and intensity of a developing storm, can have a very significant impact.

Section 1.2 also shows that the analysis increments from a single datum are proportional to the error covariance of the background. For 3D-VAR, this error covariance is designed to be nearly identical to the forecast error covariances used in the conventional OI (Heckley et al., 1992). The OI covariances are themselves fairly homogeneous and isotropic in the horizontal, with simple correlations in the vertical and between variables (Shaw et al., 1987; Undén, 1989; and references therein). In our 4D-VAR experiments the background covariances used at t_0 are identical to the constant in time 3D-VAR background covariances. In 4D-VAR, these covariances evolve implicitly, as described in Section 1.2, becoming extremely complex by t_n.

2.1 A height observation at 250 hPa.

In this experiment and in the experiment of Section 2.2, the background x_b is a 6 hour forecast, taken from a T63 OI assimilation cycle, valid at 00 UTC 15 October 1987. We chose this situation for the rapid evolution of the dynamics during the period of interest and which was reasonably captured by our T63 adiabatic forecast model (see Thépaut et al. 1993b). In particular, the vertical tilt of the low between the surface and 500 hPa, typical of a rapidly intensifying baroclinic situation, was well represented.

In the assimilation experiment we include only a single geopotential height observation located in the trough at 250 hPa (5°W–44°N) at the end of the period. The observation increment (the difference between the observation and the forecast made from the background x_b) is −70 meters, with an expected standard deviation of 12 meters. The minimization procedure is allowed to continue until the norm of the gradient of J is reduced by a factor of 1000.

Fig. 1 shows the geopotential height and wind analysis increments at the end of the assimilation period for 1000 (a), 850 (b), 500 (c) and 250 hPa (d). In the context of these experiments the analysis increment is the difference between two forecasts, one made from initial conditions x_0 and one from x_b, during the analysis time period. Clearly the analysis increments are not isotropic. While the maximum amplitude of −76 m is obtained at 250 hPa in the vicinity of the observation, there is an important west-east propagation of the information consistent with the dynamics of the model for this situation, leading to a second extremum of opposite sign (+39 m) near 20°W–40°N. Both extrema extend vertically down to 850 hPa. The vertical tilt of the positive extremum between 850 and 500 hPa is consistent with lower troposphere baroclinic instability of this meteorological situation.

As a comparison to the 4D-VAR results we perform a simple equivalent 3D-VAR data assimilation. Having only one observation at the end of the assimilation period, the analysis differs from the forecast only at this time. The resulting increments (Fig. 2) correspond exactly to the spatial structure of B. When compared with Fig. 1 and the evolution of the dynamics on this situation, one can see that isotropic and barotropic covariance functions are poorly adapted for such a meteorological situation. However, as we have noted, the covariances implied by the 4D-VAR are also imperfect. For example, because of the assumption of a perfect model, there may be meteorological situations for which the model and hence the 4D-VAR covariances are also incorrect. This is likely to be the case on this situation where the diabatic effects had an important contribution to the cyclogenesis, whereas the assimilating model we used is mainly adiabatic.

The 4D-VAR method, being a smoother, spreads the data influence both forward and backward in time. The 4D-VAR increments 24 hours before the observation are shown in Fig. 3. These increments at the initial time are quite small, within the uncertainty of our best analysis, and similar in magnitude to the data misfit at the final time. One can see that the increments propagate horizontally with basic state steering current. The negative extremum at 500 hPa at t_n is 20° east of that at t_0. In addition to the baroclinic signature in the lower troposphere and the eastward horizontal advection, we note that the perturbation propagates vertically with a maximum amplitude shifting from 400 hPa (not shown) to 250 hPa during the 24 hour period.

Note that the single height observation leads to balanced height and wind analysis increments at all times. The mass-wind balance at t_0 is a result of using a background covariance B based on a balance relationship. This mass-wind balance is then preserved by the model dynamics.

Thépaut et al. (1993b) have also compared the 4D-VAR increments to the fastest growing perturbations of this particular meteorological situation, finding out a certain visual agreement between the shape and the evolution of the most unstable mode and of

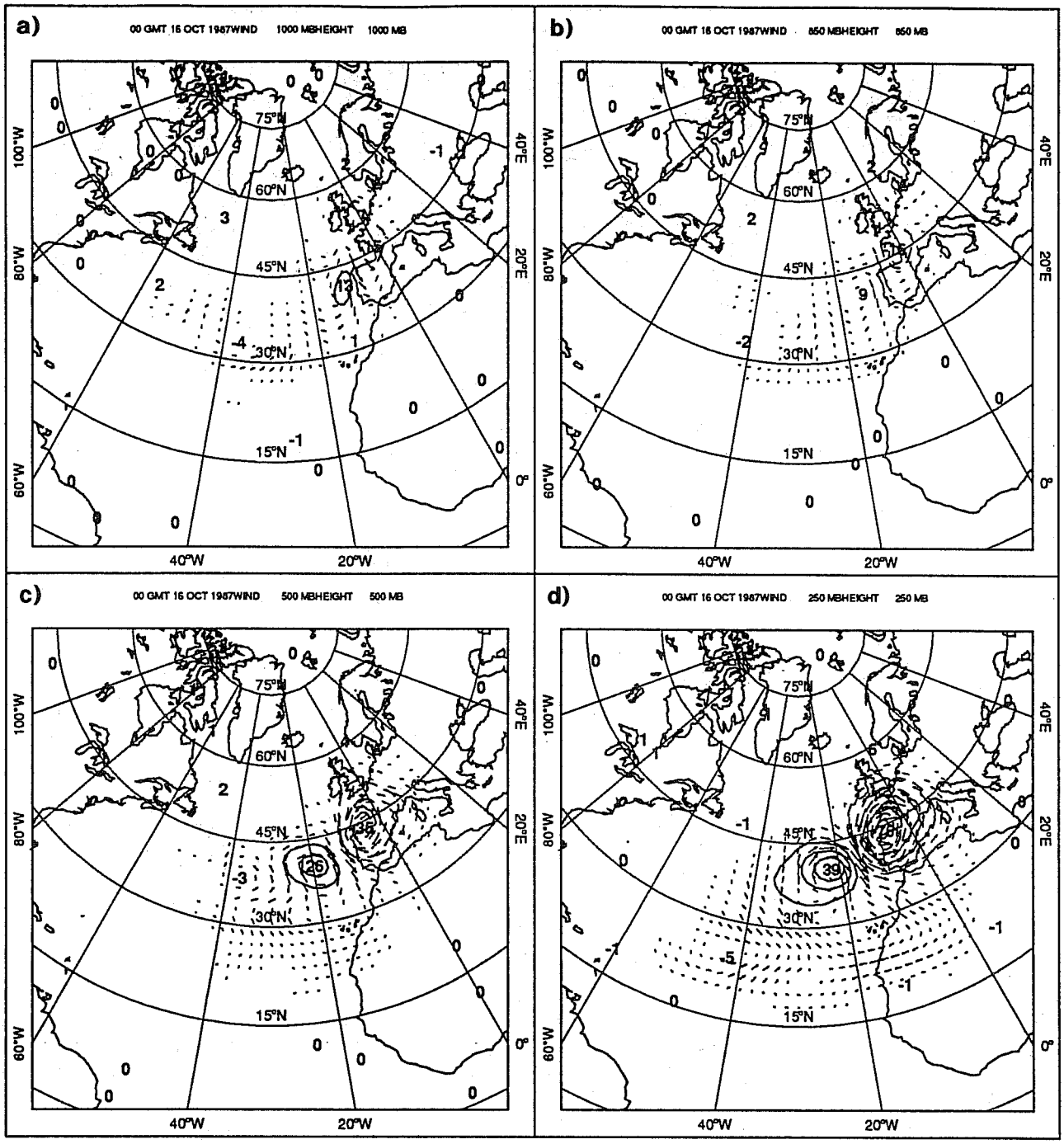

Fig 1 The 4D-VAR analysis increments (analysis - background), at the end of the 24 hour assimilation period, for geopotential height and wind at 1000 (a), 850 (b), 500 (c) and 250 hPa (d), corresponding to a single height observation at 250 hPa. Contour interval: 10 m.

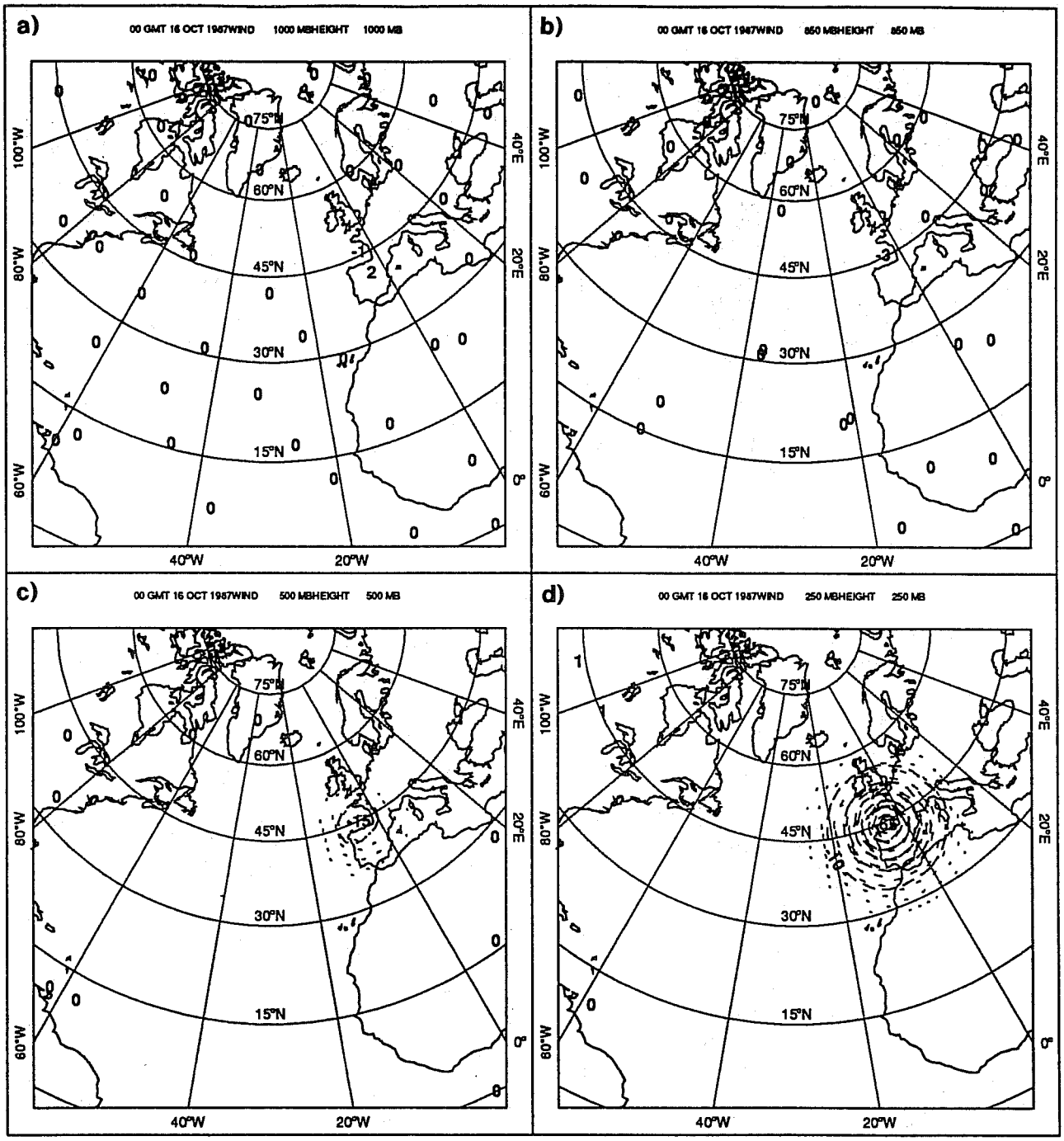

Fig 2 As in Fig 1 but the 3D-VAR analysis increments at the end of the assimilation period. Contour interval: 10 m.

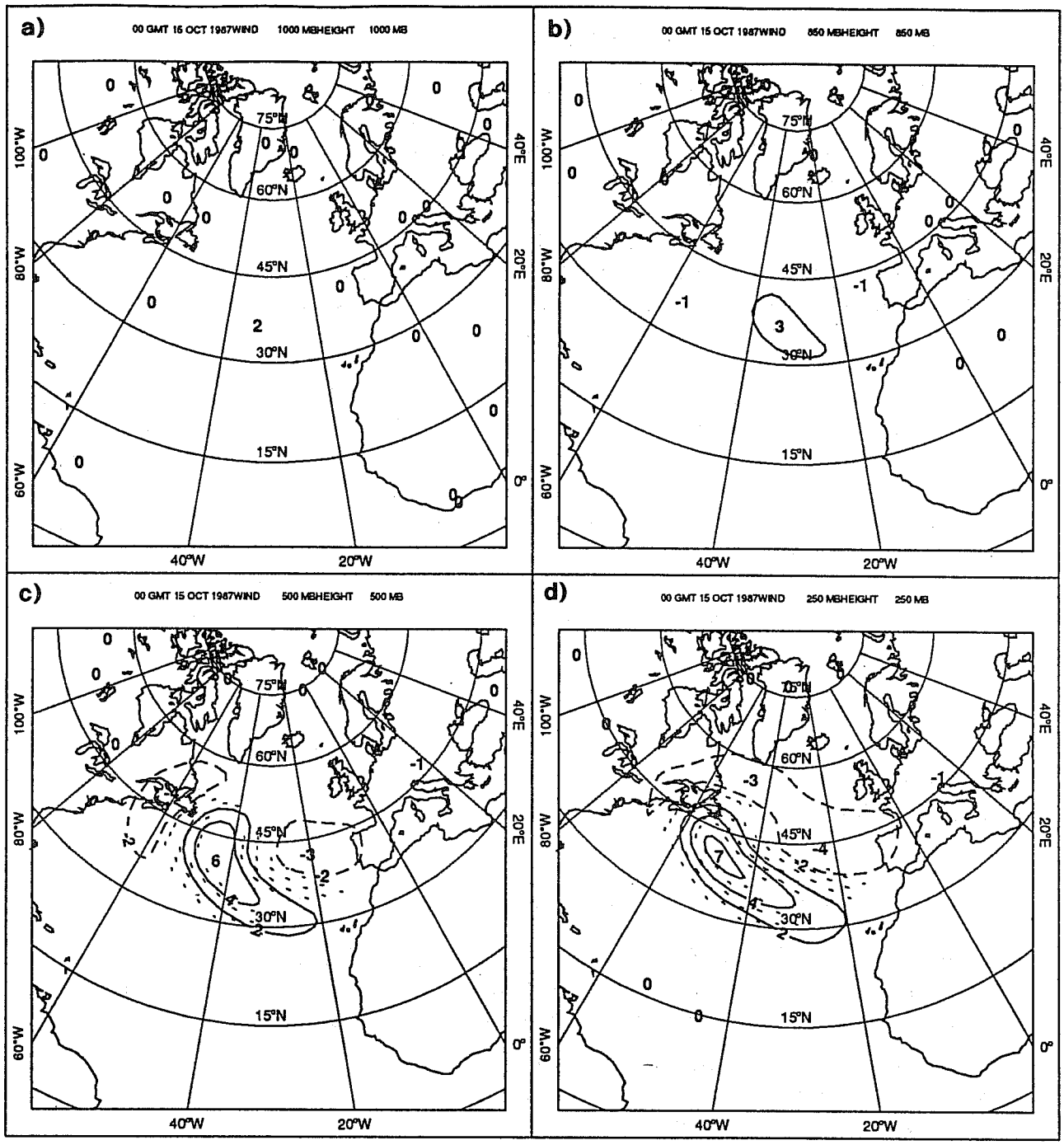

Fig 3 As in Fig 1 but the 4D-VAR analysis increments at the beginning of the assimilation period. Contour interval: 2 m.

the 4D-VAR solution over this assimilation period.

2.2 A wind observation at 1000 hPa.

This experiment parallels that of Section 2.1, except that here a single zonal wind observation is inserted at 1000 hPa. The observation location is again 5°W–44°N. The u-wind increment is 20 m/s. The observational standard deviation is 3 m/s. The resulting analyses are presented in Figs. 4, 5 and 6, which are analogous to Figs. 1, 2 and 3 presented in Section 2.1.

First considering Fig. 4, the impact is largest at 250 hPa, the level of the maximum amplitude of the optimal mode, not at 1000 hPa, the level of the observation. Also the pattern of the 4D-VAR analysis increments at 250 hPa are very similar to the previous case, but shifted a few hundred km eastward. As in Fig. 1, the dipole pattern at 250 hPa persists in the vertical, but now rotates counterclockwise with increasing pressure, completing the near quarter turn necessary to match the wind observation. The decay of amplitude with increasing pressure is less in this case. The 3D-VAR results (Fig. 5) again faithfully represents the simple background covariances. The largest 3D-VAR impacts are restricted to the levels near the data level.

At the initial time, the 4D-VAR analysis increments (Fig. 6) are quite different than in the case of the height observation. Since that data location does not match the location of the maximum amplitude of the optimal modes, a larger initial amplitude is required. The vertical structure of the initial perturbation is much more complex, with a positive extremum at 500 hPa and a negative extremum at 850 hPa. The patterns at these two levels are similar in shape and amplitude but of opposing sign. At other levels, particularly at 1000 hPa, increments are small.

These "one single datum" experiments show the ability of 4D-VAR to implicitly use flow-dependent structure functions (in this particular case strongly baroclinic) and to transfer accordingly information from a surface observation in the vertical.

3 An example of multivariate analysis in 4D-VAR

This feature of 4D-VAR, intrinsically due to its temporal dimension can be illustrated with a simple 1D advection model. We will show in sections 5 and 6 a "real-size" (full atmospheric model, real observations) demonstration of this phenomenon.

Let X the control variable be (u, q) with
$u = u(x,t)$ = wind over a periodic domain $[0, L]$
$q = q(x,t)$ = any passive tracer
We assume that the evolution equations are :

$$\frac{\partial u}{\partial t} + u\frac{\partial u}{\partial x} = \nu\frac{\partial^2 u}{\partial x^2} \tag{5}$$

and

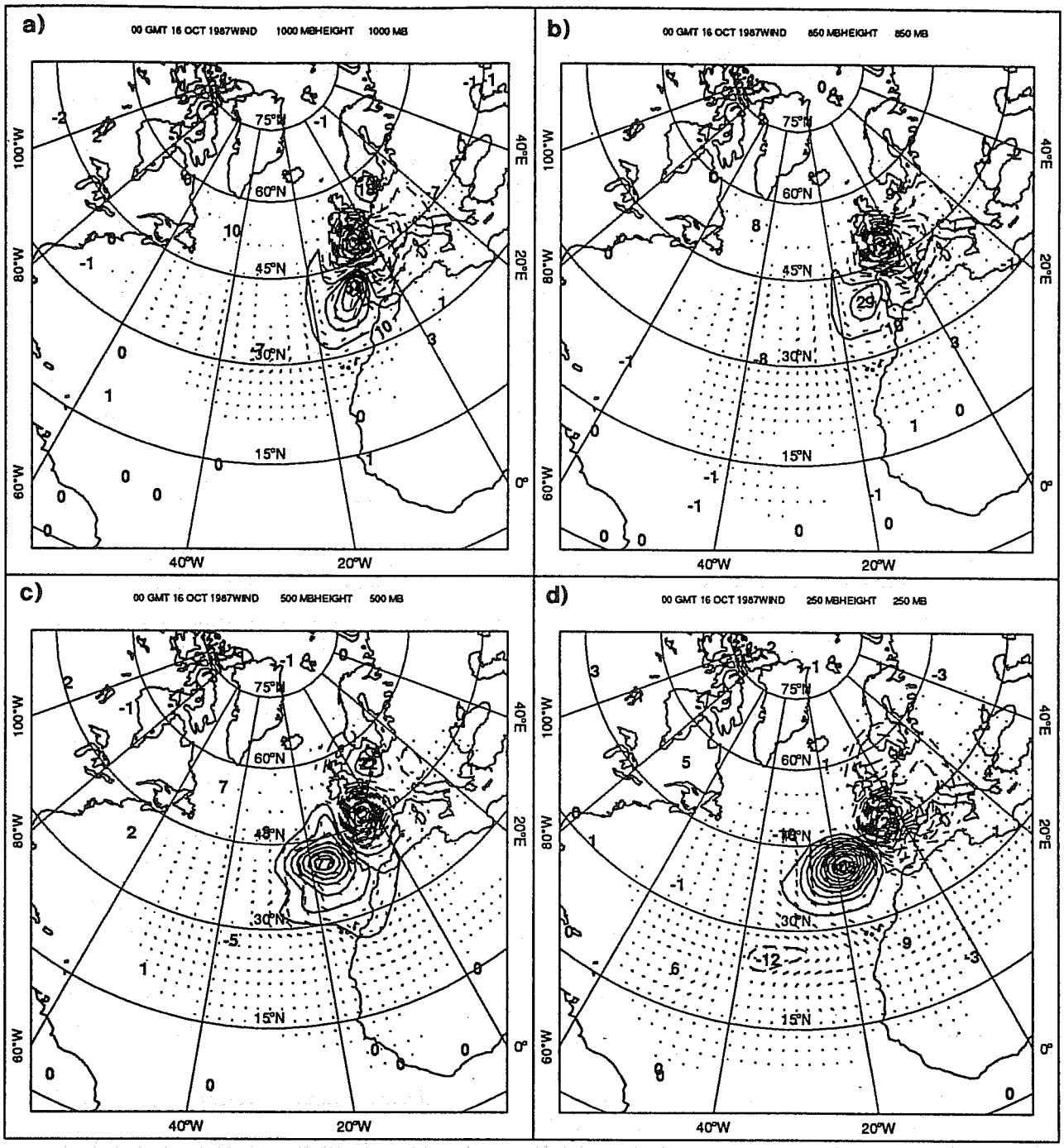

Fig 4 The 4D-VAR analysis increments (analysis - background), at the end of the 24 hour assimilation period, for geopotential height and wind at 1000 (a), 850 (b), 500 (c) and 250 hPa (d), corresponding to a single wind observation at 1000 hPa. Contour interval: 10 m.

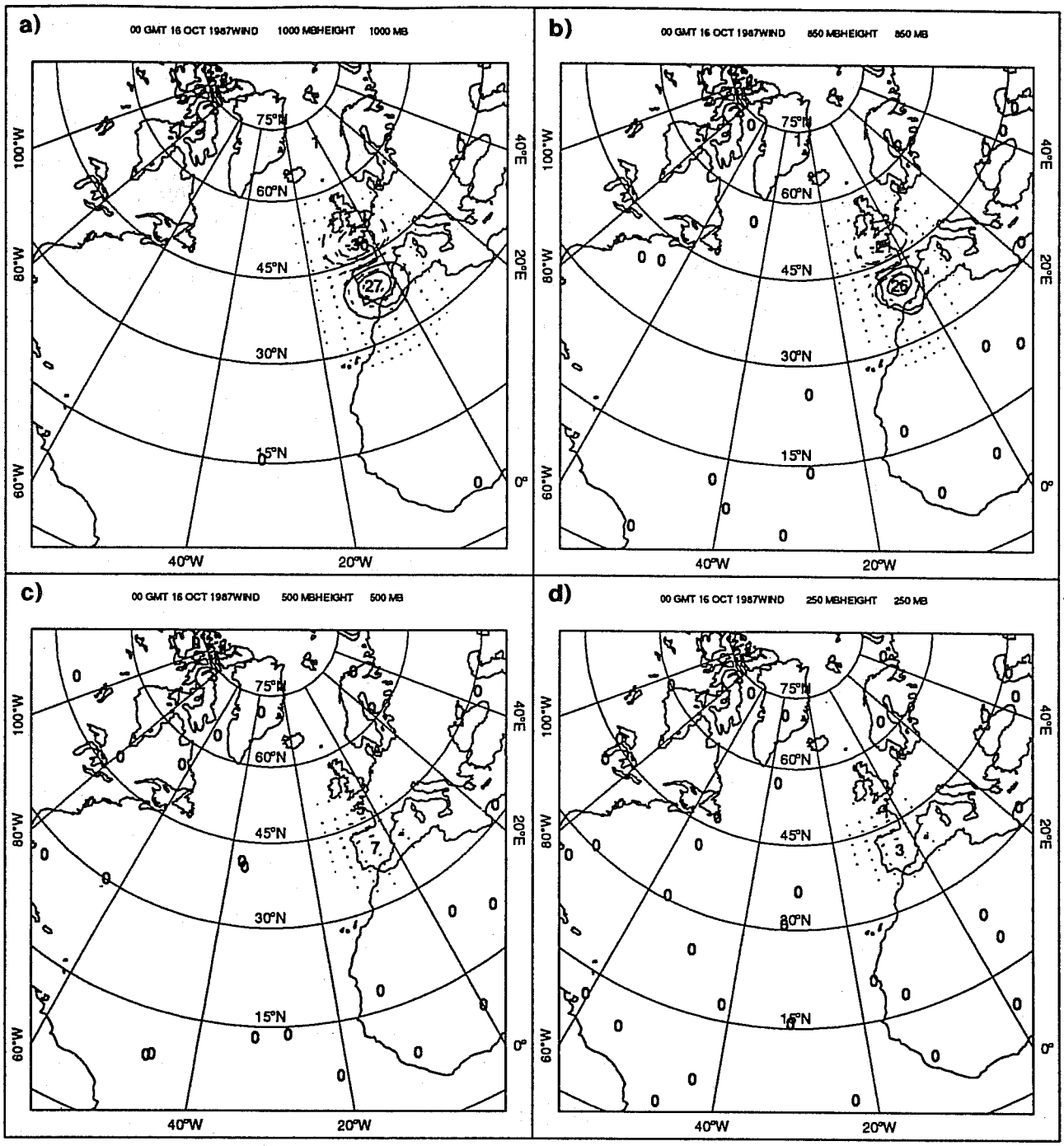

Fig 5 As in Fig 4 but the 3D-VAR analysis increments at the end of the assimilation period. Contour interval: 10 m.

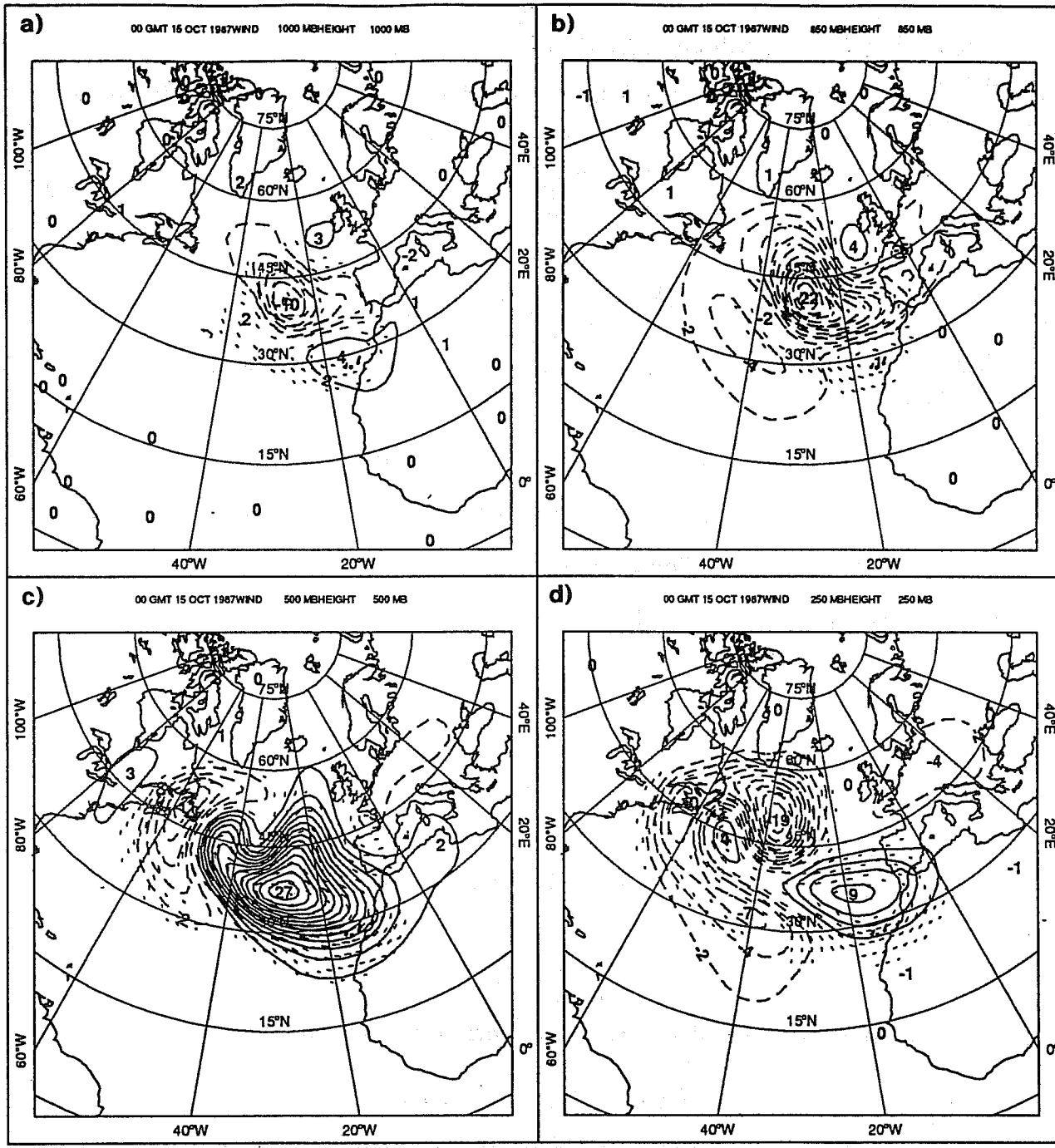

Fig 6 As in Fig 4 but the 4D-VAR analysis increments at the beginning of the assimilation period. Contour interval: 2 m.

$$\frac{\partial q}{\partial t} + u\frac{\partial q}{\partial x} = 0 \tag{6}$$

where ν is a positive diffusion coefficient.

For a given solution $(u(x,t), q(x,t))$, we can derive the TL equations for perturbations δu and δq:

$$\frac{\partial \delta u}{\partial t} + \frac{\partial (u\delta u)}{\partial x} = \nu\frac{\partial^2 \delta u}{\partial x^2} \tag{7}$$

and

$$\frac{\partial \delta q}{\partial t} + u\frac{\partial \delta q}{\partial x} + \frac{\partial q}{\partial x}\delta u = 0 \tag{8}$$

Defining an inner product for velocity and passive tracer fields defined on the spatial domain $[0, L]$:

$$< X_1, X_2 >= \int (u_1 u_2 + q_1 q_2) dx \tag{9}$$

(we suppose here for the sake of simplicity that the variables are dimensionless)

and introducing now the adjoint variable $X' = (\delta' u, \delta' q)$

we can derive the adjoint equations of 7 and 8 :

$$-\frac{\partial \delta' q}{\partial t} - \frac{\partial (u\delta' q)}{\partial x} = 0 \tag{10}$$

$$-\frac{\partial \delta' u}{\partial t} - u\frac{\partial \delta' u}{\partial x} - \nu\frac{\partial^2 \delta' u}{\partial x^2} + \frac{\partial q}{\partial x}\delta' q = 0 \tag{11}$$

(see Talagrand 1988).

Assuming now that q (and only q) is observed over the all domain, we can build the following cost function :

$$J = \frac{1}{2}\int\int_D (q - q_{obs})^2 dx dt \tag{12}$$

A perturbation δq will lead to a first-order variation of the cost-function :

$$\delta J = \int\int_D (q - q_{obs})\delta q dx dt \tag{13}$$

To compute the gradient of the cost-function with respect to the initial conditions $X_0 = (u_0, q_0)$ we integrate :

$$-\frac{\partial \delta' q}{\partial t} - \frac{\partial (u\delta' q)}{\partial x} = q - q_{obs} \tag{14}$$

$$-\frac{\partial \delta' u}{\partial t} - u\frac{\partial \delta' u}{\partial x} - \nu\frac{\partial^2 \delta' u}{\partial x^2} + \frac{\partial q}{\partial x}\delta' q = 0 \qquad (15)$$

starting from :

$\delta' q_n = 0$

$\delta' u_n = 0$

It is clear from (15) that $\nabla_{u_0} J = \delta' u_0$ contains information from the observations q_{obs} (coming from the last term of the left hand side of the equation).

In other words, due to the temporal dimension involved in 4D-VAR, information on the q field is transferred to the wind field through the dynamics.

This can have important consequences for the use of the remotely sensed observations. In fact, an improvement of the wind (which is poorly observed directly specially in the tropics) analyses can be expected from the observation of quantities like humidity or total ozone measurements. We will discuss further this point in the next sections.

4 Impact of ERS1 scatterometer σ^0 in 4D-VAR.

We describe here the first trials of using ERS1 scatterometer data whithin a 4D-VAR framework. The reader is referred to Thépaut et al. (1993b) for a thorough description of the experiments.

The result that the impact of a surface wind observation can increase with height (Section 2.2) suggests that the impact of scatterometer observations may be substantial in 4D-VAR. Two 4D-VAR assimilation experiments were performed for the 24 hour period 12 UTC 30–31 December 1991. As mentioned in the Introduction a violent storm struck the coast of Norway 24 hours later. The first experiment, referred to as CONTROL, uses all conventional upper air observations. Vasiljevic et al. (1992) describe the handling of these observations within the IFS system. A second experiment, referred to as SCATT, is identical to CONTROL except that scatterometer σ^0 observations are added as described in the next section.

4.1 The scatterometer observations cost function.

We present 4D-VAR analyses with and without C band scatterometer data from the ERS1 satellite (Francis et al., 1991). Scatterometers are active radars which respond to the roughness of the ocean surface in the centimeter range principally via Bragg scattering. The measured physical quantity is radar backscatter, referred to as σ^0. Measurements of σ^0 show a strong dependence on wind speed and direction (Schroeder et al., 1982). In conventional scatterometer data processing, several collocated σ^0 measurements may be used to retrieve wind vectors (Jones et al., 1982). The retrieval is however ambiguous (Price, 1976). A further spatial filtering or reference to an *a priori* wind field is necessary

(Schultz, 1990). To use the σ^0 data within 4D-VAR we simply add a new observation cost function. In this way the 4D-VAR approach combines the scatterometer wind retrieval and ambiguity removal problems with all other available information, including other types of observations and other constraints. The scatterometer cost function is

$$J_{scat} = \frac{1}{2}(H_\sigma(x_0) - \sigma^0)^T O_\sigma^{-1}(H_\sigma(x_0) - \sigma^0). \tag{16}$$

In our experiments, the operator H_σ is composed of:

- A forecast model to advance the model state in time from t_0 to t_n.
- An inverse spectral transform from spectral to grid-point space.
- A horizontal interpolation from the grid-points to the observation locations.
- A vertical interpolation to evaluate neutral stability wind at the reference height of the scatterometer (10 m) from the wind at the lowest model level.
- A model function to compute the σ^0 that would be observed given the neutral stability wind.

The adjoint of all these operators is of course needed to compute the gradient of J_{scat} with respect to the control variable. In the present experiments the horizontal interpolation is linear in latitude and longitude. The vertical interpolation is based on a simple logarithmic wind profile with no stability correction. (However, provisions have been made to use the full boundary layer formulation in evaluating J_{scat}. In this case the 10 m neutral wind is a function of the lowest model layer wind, temperature and specific humidity, and the surface pressure and temperature.) The model function is the prelaunch CMOD2 (Long, 1991) as tuned by Stoffelen and Anderson (1992a).

We treat the scatterometer data as if the observational errors are uncorrelated. In fact they are correlated, but by thinning the data to 100 km resolution we eliminate most of the correlations. In addition, we adjusted our model of the observational standard deviations to take into account the first order effect of the remaining correlations. The observational standard deviation is usually given in terms of K_p, the expected standard deviation of σ^0 expressed as a fraction. That is the observational standard deviation is $K_p\sigma^0_{observed}$. K_p should account for several error sources, namely communication noise, radar equation and model function uncertainties and representativeness error. Large values of K_p generally occur for low wind speed, small incidence angles and small values of σ^0. Here we use a model of K_p, polynomial in $\ln(\sigma^0)$ and incidence angle, developed for the model function and analysis resolution used. The calculated values of K_p range from 0.1 to 0.3. With these simplifications, J_{scat} takes the form

$$J_{scat} = \frac{1}{2}\sum_{\sigma^0} \frac{(\sigma^0_{model} - \sigma^0_{observed})^2}{(K_p\sigma^0_{observed})^2} \tag{17}$$

Both (16) and (17) are used for either 3D-VAR or 4D-VAR. Within the 3D-VAR and 4dVAR configurations in the IFS system, the handling and use of the scatterometer σ^0 parallel in many respects the handling and use of TOVS radiance data (Pailleux et al., 1991 and Andersson et al., 1993).

4.2 Numerical results.

This case is chosen for study because of the intrinsic interest of the 1992 New Year's Day storm and because a preliminary study of the impact of scatterometer winds in the operational OI assimilation had previously been performed at ECMWF for the period from 00 UTC 26 December 1991 through 2 January 1992 (Hoffman, 1993). The conclusions of that study were:

- The impact of the data on the assimilation is weak.
- The analysis draws to the data without producing associated changes to the mass field.
- The analysis changes decay in the subsequent 6 hour forecast.
- The ambiguous nature of the scatterometer winds requires strong quality control.

The present experiment tests the performance of 4D-VAR for the same situation, although with a simplified forecast model. The advantage of the variational approach is that it embeds the ambiguity problem in a large data fitting problem which includes other observations, a background constraint based on balanced error covariances and the model dynamics. The last two factors lead necessarily to a dynamically consistent use of the data.

In both CONTROL and SCATT we add a weak constraint on the gravity waves as in Courtier and Talagrand (1990). Also in both cases the minimization is stopped after 30 iterations. In SCATT, the σ^0 are quality controlled in the sense that they are rejected if the sea surface temperature at the observation location is less than 274.5 K or if the analyzed 10 m wind speed (from the SCATT experiment of Hoffman (1993)) is less than 4 m/s.

In spite of the complexity of J_{scat}, no convergence problems are encountered during the minimization. In the SCATT assimilation, the distance between the model solution and the σ^0 data decreased substantially after 30 iterations (by a factor of 2.2 for the normalized standard error) while the fit of the other observations is hardly changed relative to that of CONTROL. During the minimization process, the part of the cost function due to the observations decreases rapidly at first and then more slowly. The full cost function has the same quasi-exponential decaying behavior because the observations dominate the cost function. The part of the cost function due to the background is initially zero and grows during the course of the minimization, but is always an order of magnitude smaller than the part due to the observations. The part of the cost function due to the constraints remains fairly constant during the minimization but is smaller still, roughly two orders of magnitude smaller than that due to the data.

The data used in the present experiment in addition to the ERS1 σ^0 observations are radiosonde, pilot balloon, aircraft, and satellite cloud track wind observations; drifting buoy surface pressure observations; and radiosonde temperature and humidity observations. Conventional surface observations and satellite temperature and humidity profiles are not used. The treatement of the observations, other than scatterometer observations,

in our experiments is the same as in Thépaut et al. (1993a). In our experiments the scatterometer data are the most numerous data at the surface, since the number of drifting buoys is small and the conventional surface observations are not used. Also at times other than the four synoptic times, the scatterometer data are often the most numerous data type, even exceeding the total of all other data occasionally during the assimilation. It should be noted however that these data cover only a small geographical area since they are confined to a few swaths about 500km wide. In the Southern Hemisphere and Tropics the scatterometer data and cloud drift winds dominate the other data types. In the vertical the number of radiosonde and pilot balloon observations is a maximum at 850 mb, decaying slowly throughout the troposphere and lower stratosphere, while aircraft reports concentrate around 250 hPa, and the majority of satellite winds occur at 850 hPa. Typical temporal and geographic data coverage is presented by Thépaut et al. (1993a) (Table 1 and Figure 1).

Fig. 7 presents the mean sea level pressure field for the 4D-VAR SCATT and CONTROL assimilations and the difference of the two at the end of the assimilation period. As expected, the impact is large in the Southern Hemisphere, with differences of up to 10 hPa southwest of Africa. Substantial differences can also be observed in the Northern Hemisphere, especially in the North Atlantic. Generally the σ^0 data strengthen the activity of the effected systems. This can be seen, for example, southwest of Africa, southwest of South America, and southwest and northeast of Iceland. At 500 hPa (not shown) the impact is still quite large. Again, the systems are intensified in the SCATT assimilation.

The area near Iceland is of particular interest since at 12 UTC 31 December 1991, the New Year's Day storm was forming southwest of Iceland. Subsequently, this storm grew and rapidly evolved, striking the Norway coast 24 hours later. Also there is fairly good σ^0 data coverage over this area at the end of the assimilation period. We have compared the performances of SCATT and CONTROL analyses with several manual operational analyses made by the Icelandic, Norwegian and British Meteorological services. Fig. 8 presents the analyzed mean sea level pressure, valid at this time, over the North Atlantic produced by CONTROL (a), SCATT (b), the operational ECMWF T213 analysis (c) and the manual analysis of the UK Meteorological Office (d). West southwest of Iceland, SCATT strengthens the low with a substantial increase of the pressure gradient at (25°W–50°N). This seems consistent with the operational ECMWF analysis. More questionable is the presence of the ridge between Greenland and Scandinavia and the two lows north of Iceland in both 4D-VAR runs and especially in SCATT which creates two isolines at 972 hPa. This low pressure area is less marked in the operational ECMWF analysis. The solution adopted by the UKMO analysts is somewhere in between.

Thépaut et al. (1993b) also showed that evidence in support of the 4D-VAR analyses came from the TOVS AVHRR imagery, indicating a vortex northeast of Iceland at 12 UTC and intensifying in the next 6 hours. This feature was better represented in the 4D-VAR assimilations than in the operational analysis. Furthermore, the σ^0 data have a beneficial impact, strengthening the analyzed low.

They also showed that despite the crudeness of the model (T63 resolution, lack of physics) used in the assimilation experiments,the impact of the σ^0 data was persisting in the short-range forecast, valid 00 UTC. These results were quite a bit more encouraging

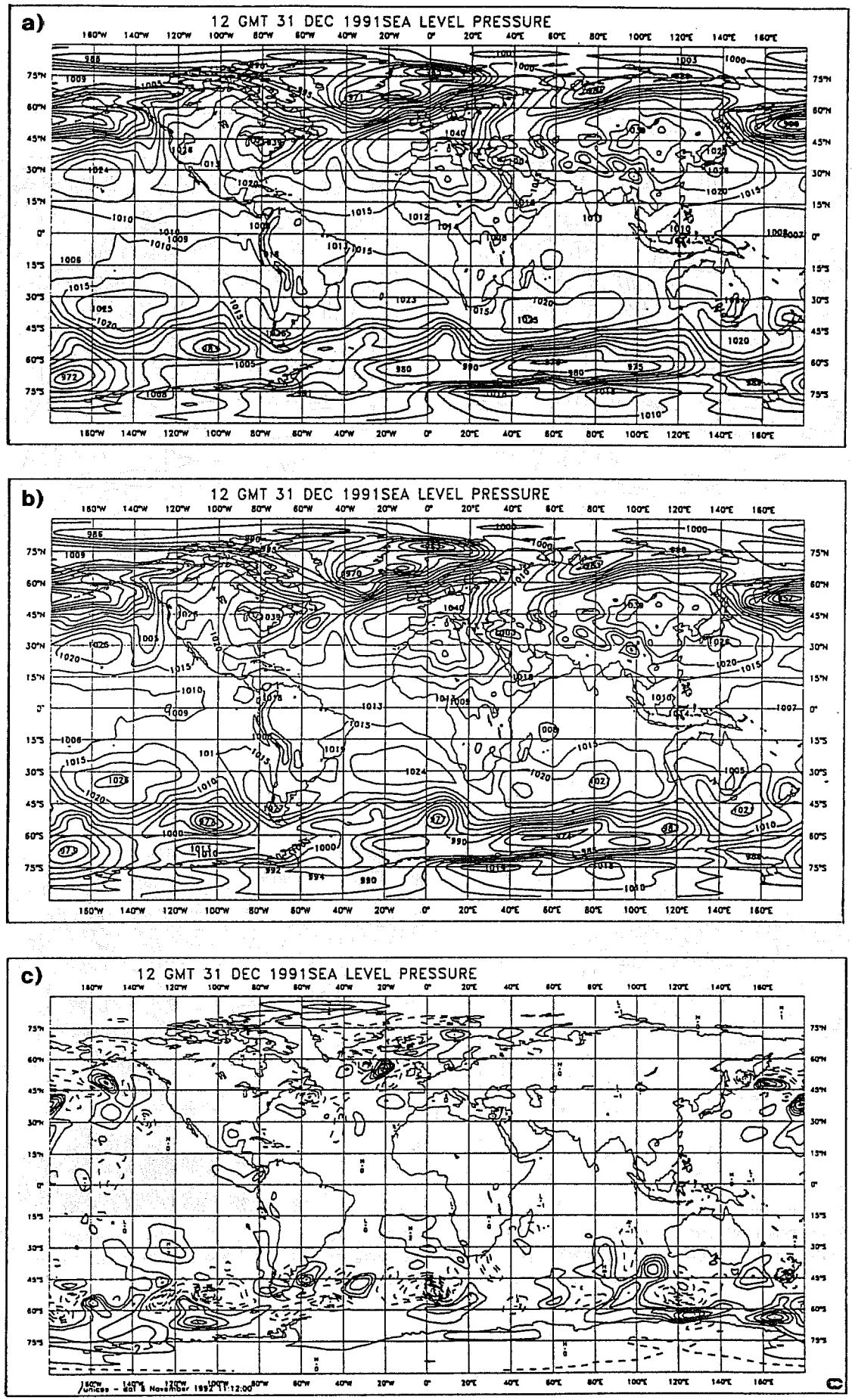

Fig 7 Mean sea level pressure at the end of the assimilation period (12 UTC 31 December 1991) for (a) the CONTROL assimilation, (b) the SCATT assimilation and (c) for SCATT - CONTROL. Contour intervals: 5 hPa for the fields and 1 hPa for the differences.

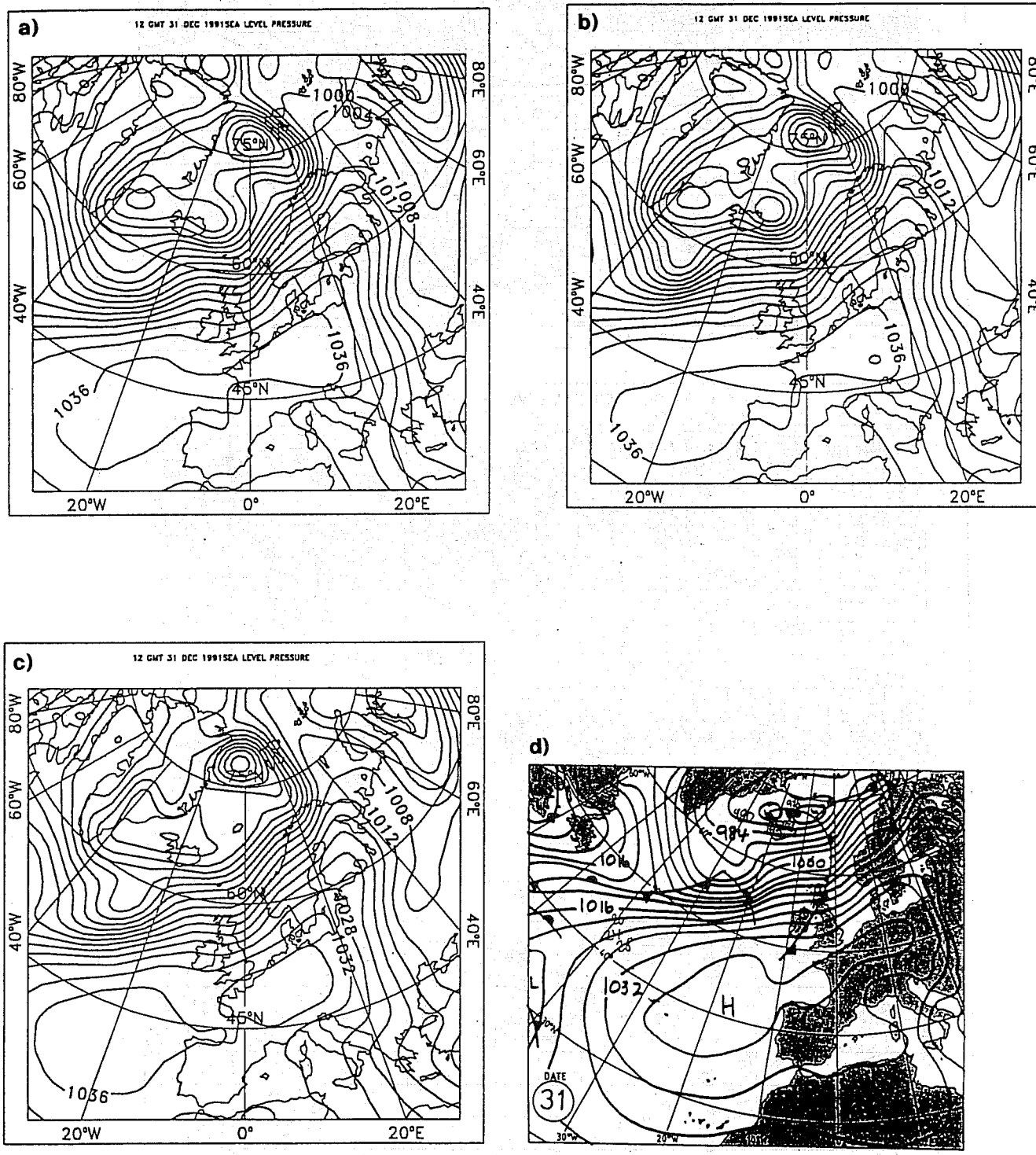

Fig 8 Mean sea level pressure analyses valid 12 UTC 31 December 1991 from (a) the CONTROL assimilation, (b) the SCATT assimilation, (c) the ECMWF T213 operational suite and (d) the UKMO (subjective) analysis (from Weather, 1992, Vol 47, No. 2, published by the Royal Meteorological Society). Contour interval: 4 hPa.

than the forecast results obtained by Hoffman (1993) using the scatterometer winds in the conventional OI assimilation system.

Two further assimilation experiments were run in which conventional surface observations were added to both CONTROL and SCATT. In particular 10 meter wind measurements from ships were included. The impact of the σ^0 data was not significantly changed by the presence of the surface observations.

5 Impact of TOVS radiances in 4D-VAR.

We have seen in section 3 on a toy case how it was possible to infer information on non-directly observed fields through the dynamics involved in 4D-VAR.

A "true-size" 4D-VAR experiment using TOVS radiances has been carried out to illustrate this phenomemon. This experiment is described in detail in Thépaut (1992) and Andersson et al. (1993).

One of the strong motivations to develop the "IFS/ARPEGE" Integrated Forecasting System (Pailleux, 1991) was the possibility of using directly TOVS radiances in a variational analysis (3D/4D). The problem of correlation between observation error and background error (Eyre et al. 1993) is then avoided. Furthermore in 4D-VAR, dynamical consistency is ensured with the forecast model acting as a strong constraint.

5.1 Experimental framework.

Similarly to section 4.1, the introduction of radiances leads an additional term in the cost function of the form :

$$J_{R_o} = \frac{1}{2}(H_{R_o}(x_0) - R_o)^T O^{-1}(H_{R_o}(x_0) - R_o). \tag{18}$$

In our experiments, the operator H_{R_o} is composed of:

- A forecast model to advance the model state in time from t_0 to t_n.
- An inverse spectral transform from spectral to grid-point space.
- A horizontal interpolation from the grid-points to the observation locations.
- A vertical interpolation/extrapolation to go from the model levels to the fixed pressure levels of the radiative transfer model.
- A radiative transfer model to compute the radiance R_o that would be observed given the atmospheric state x_n.

Again, the adjoint of all these operators is needed to compute the gradient of J_{R_o} with respect to the control variable.

The observation operator we have used is described in detail in Andersson et al. (1993) where TOVS radiances are assimilated in a 3D-VAR context.

The difference between 3D-VAR and 4D-VAR is that the forecast model is involved in the definition of the H_{R_o} operator.

A 4D-Var experiment was carried out in order to find out to what extent the dynamics of the forecast model, in the absence of a background term, could provide wind increments in response to TOVS information solely on the mass field. The first reason for not using background information in this experiment is that at a time, the background term of the cost-function was still at a development level. Moreover, the background information is generally much less important in 4D-Var than in 3D-Var. The three-dimensional analysis problem is under-determined unless background information is provided. In four dimensions, a strong constraint is posed by the evolution of the forecast model; the model trajectory has to stay close to the observations over a period of time, which makes it possible to ignore at low resolutions, especially if the assimilation period is long enough. The experiment presented here used TOVS from 18,208 locations over a 24 hour period as well as most conventional data (SYNOP, SHIPs, DRIBU, TEMP, PILOT, AIREP and SATOB). The resolution of the spectral model was T42-L19 (140 000 degrees of freedom). The model was used in its adiabatic version, and a combination of a weak constraint term on the tendencies of the energy in the gravity components of the model solution and a normal mode initialisation scheme was applied in the assimilation process in order to control noise (Thépaut and Courtier, 1991). A second assimilation was run with only conventional data so that the difference between the two assimilations would show the impact of TOVS in the presence of all other data.

The computation was split into one-hour time slots, but is otherwise as described in Andersson et al. (1993). Horizontal correlation of the observation error between adjacent data in separate time slots can not be taken into account. This is considered not to be a serious limitation, similar to the approximations already present in the 3D case. The minimisations were terminated at 30 iterations, although the cost function was still decreasing. Previous experiments had shown that in the absence of a background there was a tendency to draw to the data too much at the final stages of the minimisation and noise was generated. After 30 iterations the cost function had been divided by a factor of six, in both assimilations.

5.2 Impact on the mass field.

Fig. 9 represents the 500 hPa height field difference between the 4D-Var experiment using conventional and TOVS data and the 4D-Var analysis using conventional observations only. This level roughly corresponds to the peak of HIRS channels 4, 5 and 15 and MSU channel 2. The impact of TOVS radiances is mainly located in the mid-latitudes of the southern hemisphere, and more particularly over the oceans where the differences reach more than 100 m. Bearing in mind the lack of conventional data in the southern hemisphere, the horizontal distribution of the impact is as expected. It is notable that the magnitude of the increments agrees with that of the 3D-Var experiment presented in Andersson et al. (1993), although the background constraint, which is dominant in the 3D case, is absent in the 4D experiment. Also the position of the increments show a great deal of agreement with the 3D experiment, bearing in mind that there is a 24 hour time

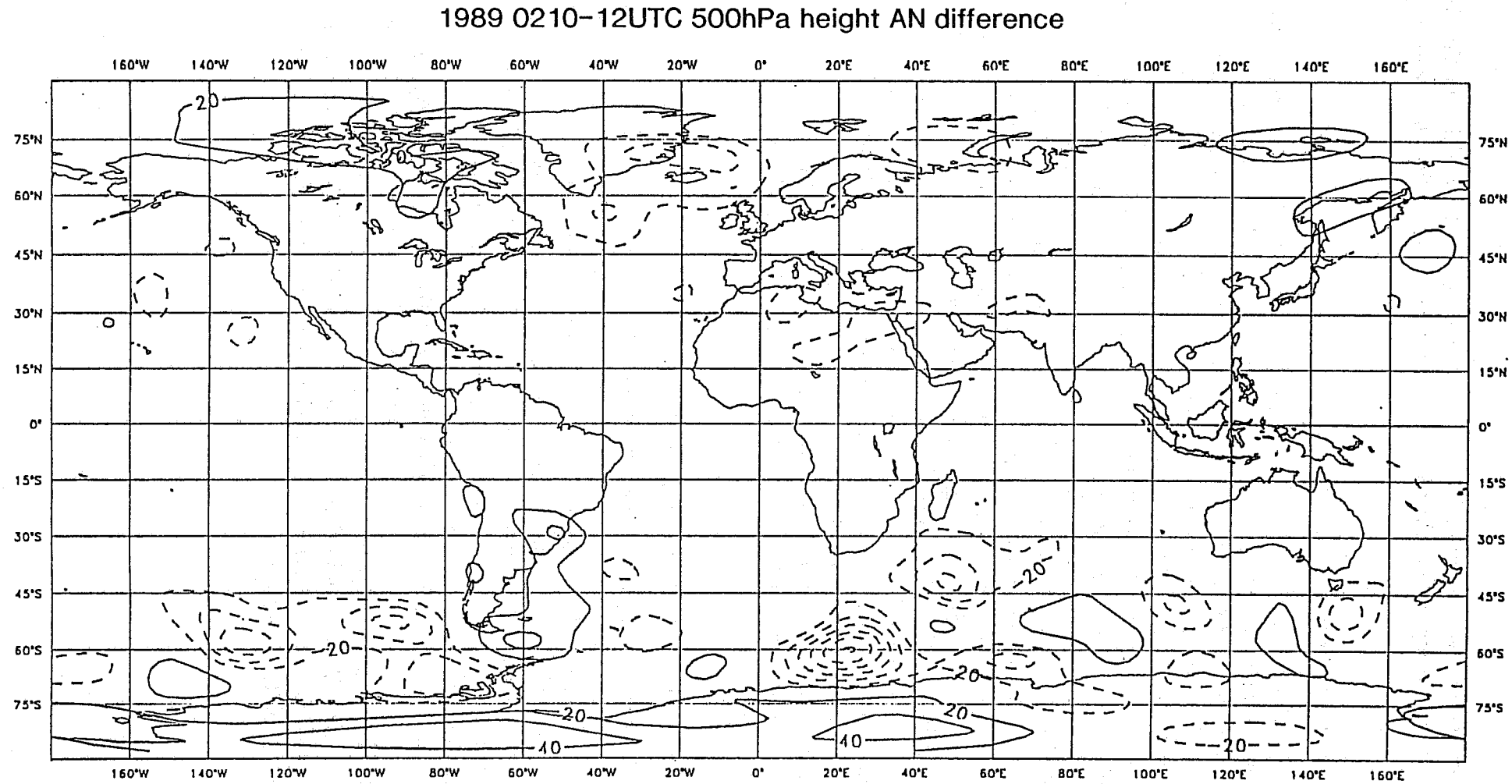

Fig 9 Geopotential differences at 500 hPa at the end of the assimilation period (890210-12UT) between 4D-VAR performed with conventional observations plus TOVS radiances and 4D-VAR performed with conventional observations only. Negative differences are dashed, and the contour interval 20 metres.

difference between the two analyses. The increments are generally positive in the ridges and negative in the troughs (not shown), they hence tend to amplify the waves in the analysis.

5.3 Impact on the wind field.

It is more interesting to look at the wind increments inferred by the use of the radiances (Fig. 10). When comparing with Fig. 9, one can notice that in the mid-latitudes the wind differences appear geostrophically related to the geopotential differences, as expected from balanced fields. This shows that the information brought by the additional observations is dynamically consistent with the model solution. In other words, the mass-wind balance information, mainly enforced by the presence of a constraint term on the gravity mode tendency and a normal mode initialisation before the model integration, has been properly transferred by the dynamics. Wind differences are also noticeable in the tropics. The location of the largest wind difference patterns correspond quite well to the locations of the humidity increments (not shown). This raised the question whether there had been an impact on the wind analysis from the humidity information in the radiances. To investigate this wind-humidity coupling, a 4D-Var experiment using TOVS data had to be rerun but excluding TOVS humidity channels HIRS-11 and 12. The new resulting 500 hPa wind difference is shown in Fig. 11. A large part of the wind increments has been wiped out, both in the tropics and in the mid-latitudes. Channels HIRS-11 and 12 are rather sensitive to temperature which is very variable in the mid-latitudes. In the tropics where the temperature field is fairly flat, the comparison between Fig. 11 and Fig. 10 clearly confirms that a large part of the wind increments is due to radiance measurements in the humidity channels.

5.4 Impact on the humidity field.

The impact of HIRS-11 and 12 on the analysed specific humidity at 500 hPa is shown in Fig. 12 on a background of the GMS infra-red cloud picture (together with corresponding wind vector differences). This can serve as a subjective verification of the humidity analysis. We can see that the two largest analysis differences appear in the areas of two active weather systems with extensive cloudiness, to the south-west of the Australian continent. The use of the the TOVS data has moved the system nearest Australia towards the west, and moistened the area around system located further to the west. The location of the two humidity maxima in the analysis that used HIRS-11 and 12 (Fig. 13) is in good agreement with the cloud picture. The drying by 0.5 g/kg to the South of Australia (Fig. 12), from 2.5 to 2.0 g/kg (Fig. 13) takes place in an area with less extensive, mostly low-level cloudiness. We conclude that the information in the TOVS humidity channels has improved the humidity analysis; the impact is subjectively in good agreement with the coincident satellite cloud image.

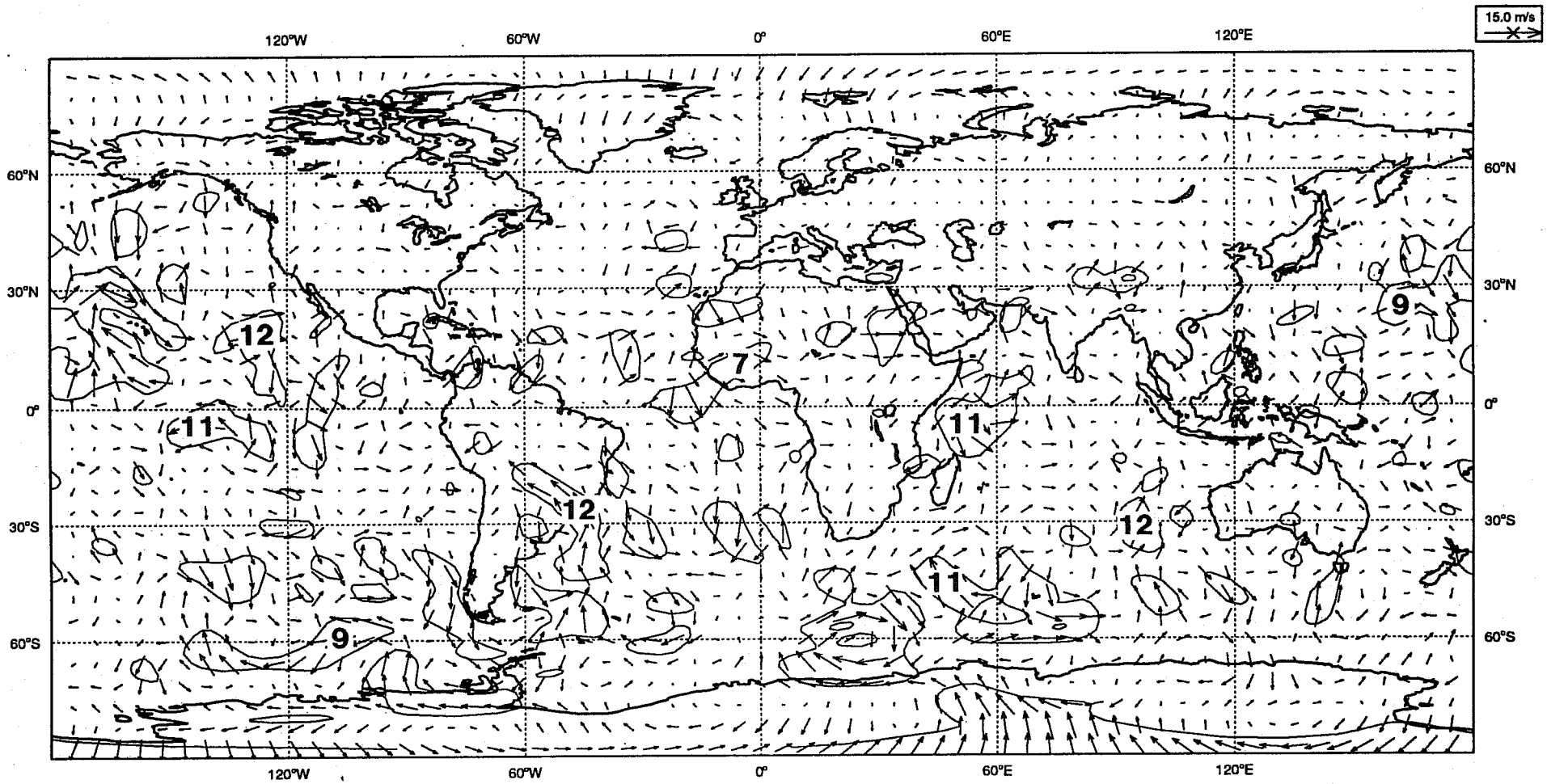

Fig 10 As Fig 9 but for the wind field. Wind speed is contoured with an interval of 5 m/s.

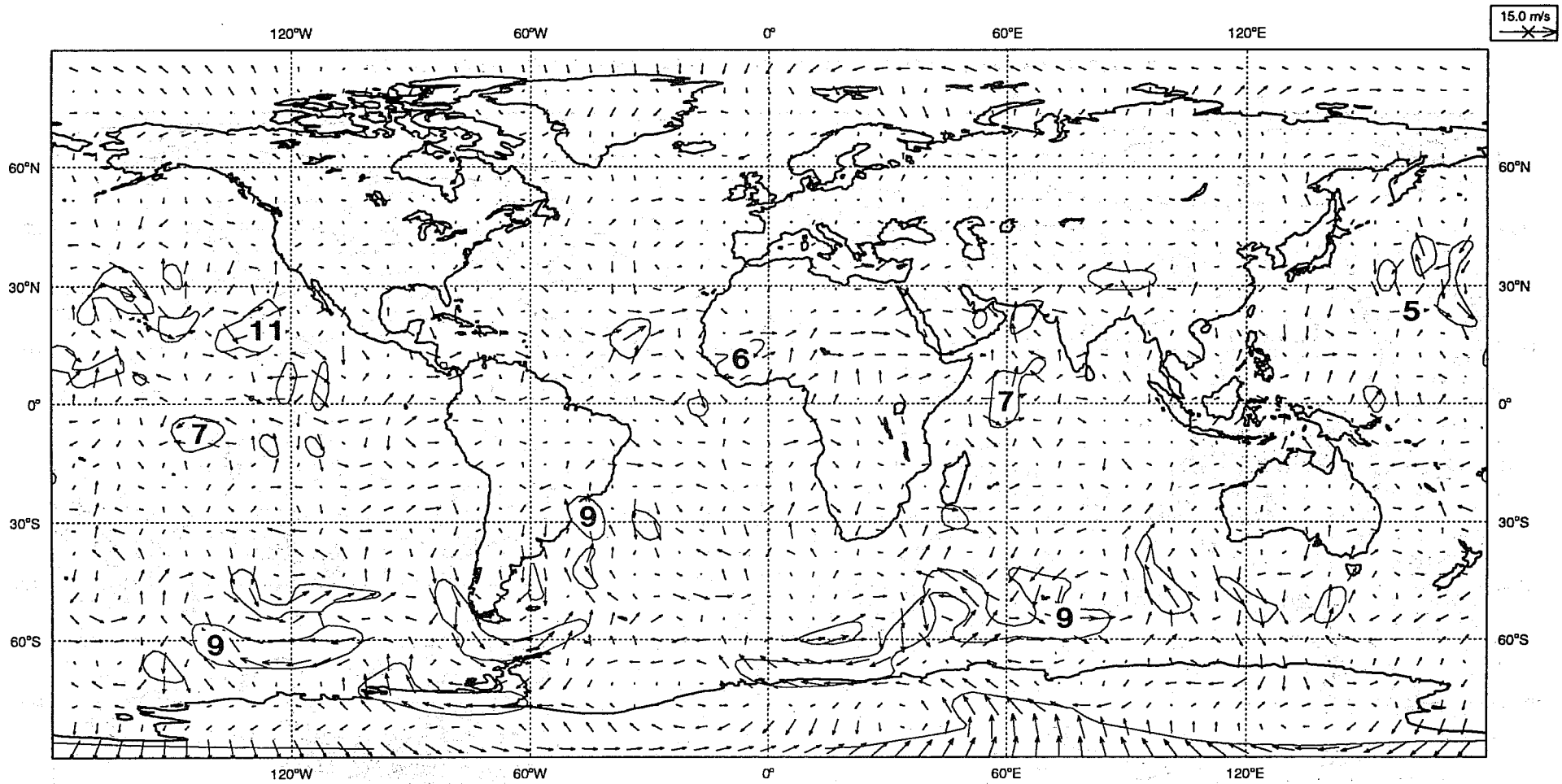

Fig 11 As Fig 10 but humidity TOVS channels HIRS-11 and 12 have been excluded from the assimilation using TOVS radiances.

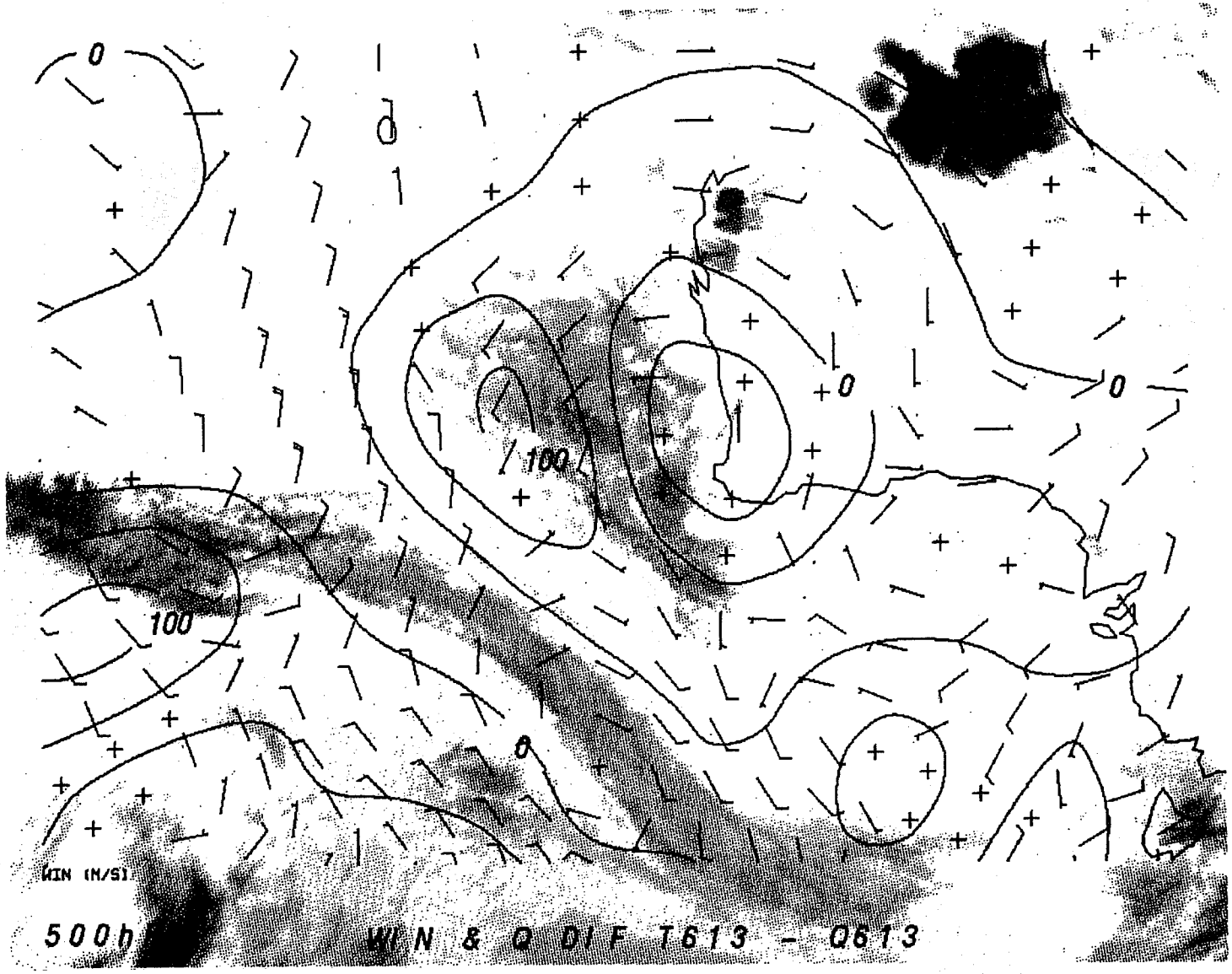

Fig 12 500 hPa specific humidity difference (contoured, in g/kg*100.) and vector wind difference (flags, long barb is 10 knots, short barb is 5 knots) at the end of the 24-hour assimilation period (890210-12 UT), between two 4D-VAR assimilations with conventional observations and TOVS radiances - one excluding HIRS-11 and 12. The plot shows the impact of using HIRS-11 and 12 - the two most humidity sensitive channels. The humidity field is contoured with an interval of 0.5 g/kg on a background of the coincident GMS infra-red cloud picture.

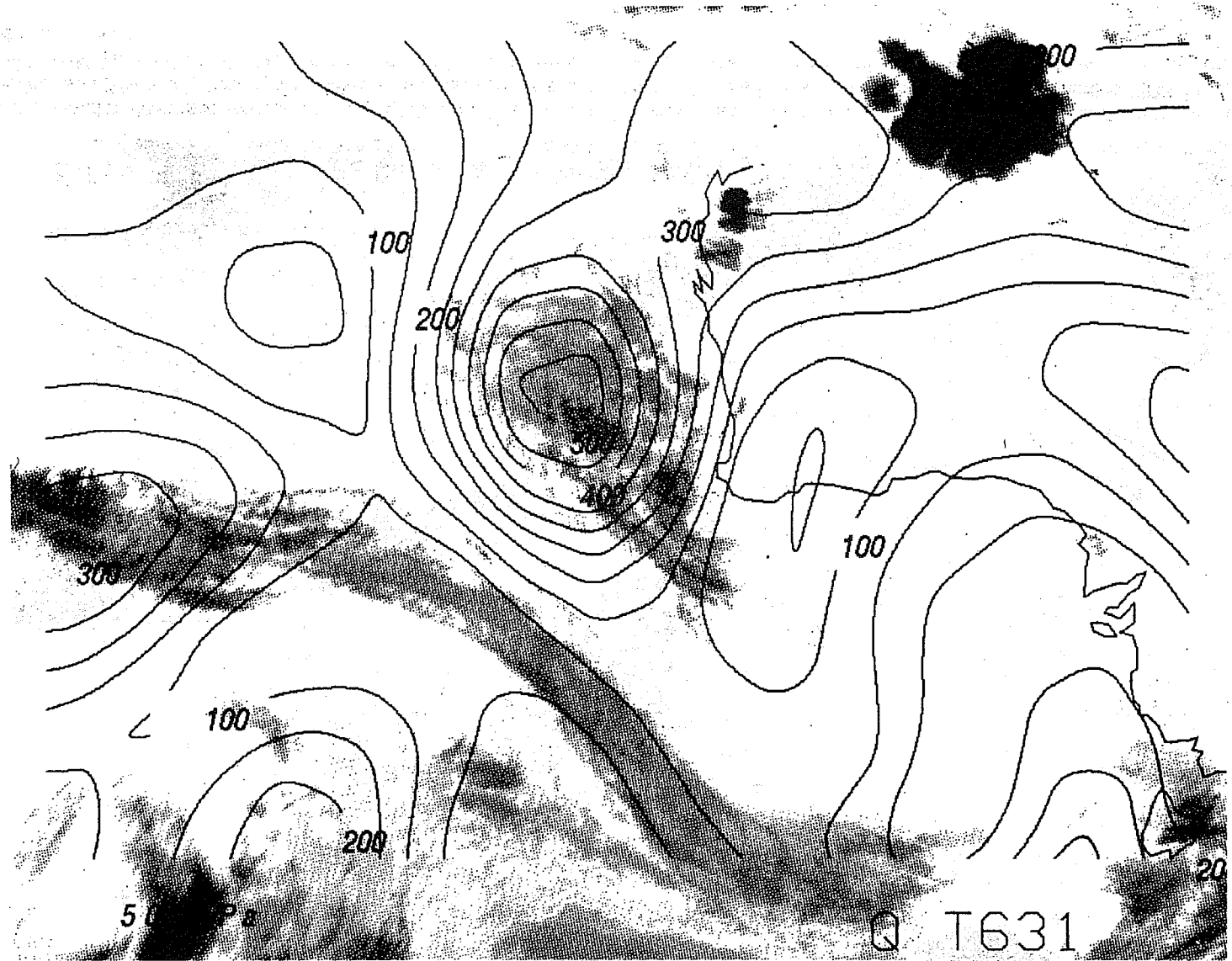

Fig 13 Like Fig 12 but the plotted field is specific humidity (in g/kg*100.) in the 4D-VAR assimilation that used conventional data and TOVS radiances, including HIRS-11 and 12.

5.5 Wind-humidity coupling.

The wind flags in Fig. 12 show the impact on the wind field from the use of HIRS-11 and 12. The largest wind differences do not necessarily coincide with the largest humidity differences – there are wind differences also in the areas in between the weather systems. Since in our experiments the humidity field behaves mostly like a passive tracer, this result, intrinsically linked to the four-dimensional nature of the assimilation, shows a nice example of how the dynamics of the model is able to infer information on an un-observed component of the flow (the wind) from remotely sensed information on the humidity field. The process could be described as a retrieval/assimilation of "water-vapour winds" from TOVS radiance data. When more realism has been introduced in the assimilating model, it is expected that this ability of 4D-Var can improve the tropical analysis.

6 Impact of SSMI pwc observations 4D-VAR.

Along the same lines as in the previous section, a 4D-VAR assimilation experiment has been carried out (Filiberti, 1993) to evaluate the ability of the system to extract the information contained in the SSMI humidity data.

6.1 Experimental framework.

The assimilations (with and without SSMI data) were performed from the 13 october 1987 12 UTC to 14 october 1987 12 UTC. Contrary to the previous section, we have not assimilated directly the radiances but the Precipitable Water Content data (PWC) available over this 24 hour period.

A rough quality control was applied to the data :

- data were excluded above 60N and below 60S (to avoid ice contamination)

- data too close to land were also rejected.

- A thinning algorithm was applied by taking one point out of five in both directions (to ensure horizontal consistency with the resolution of the model) and by rejecting the observation when the difference between the background and this observation was greater than four times the observation error standard deviation. The observational error was supposed to be 20 percent of the observed value for a pwc smaller than 25 kg/m^2 and 10 percent for a pwc greater than 25 kg/m^2.

The cost function we used contained an observational term and a background term. An additional weak constraint was imposed to ensure the solution to remain free of gravity waves. The introduction of this new type of observation leads to a new term in the observational cost-function :

$$J_{pwc} = \frac{1}{2}(H_{pwc}(x_0) - W_o)^T O_{pwc}^{-1}(H_{pwc}(x_0) - W_o). \qquad (19)$$

H_{pwc} being composed of :

- forecast model from t_0 to observation time.
- inverse spectral transform to go to grid-point space.

- horizontal interpolation to go to the observation point.
- vertical integral to compute from the profile of q the equivalent in PWC.

the observation operator is here trivial:

$$W_{model} = \int_{p_s}^{0} q dp \tag{20}$$

where p_s is the surface pressure at the observation point.

The experiment was performed with the same model as in section 4 and also at a spectral resolution of T63.

6.2 Numerical results.

We first present in Fig. 14 from Filiberti (1993), a global diagnostic of the fit of the different analyses to the observations. Panel (a) represents the value of the observational cost function for different types of conventional observations and for the Northern Hemisphere, (b) for the Tropics, (c) for the Southern Hemisphere and (d) for the satellite derived observations over the globe. The first column describes the observation type, the second column the number of pieces of information, the third column the cost function before minimisation, the fourth column the cost function after minimisation when no SSMI data were used in the assimilation and the fifth when SSMI data were actually used.

What is striking is that the fit is better for almost all types of observations and all geographical areas (except Dribus in the tropics but with a sample of only 79 observations), when SSMI PWC data are used in the assimilation. In other words, these extra observations have been used consistently with the conventional ones. This is a good sign for the data which turn out to be perfectly compatible with the usual ones, and for 4D-VAR which is able to extract properly this additional information. It is particularly encouraging to see that the fit to the satellite derived winds (see panel (d) for satellites METEOSAT and GOES W) is improved when humidity observations are put in the system.

Fig. 15 represents the PWC field obtained from the operational ECMWF analysis (panel a.), the 4D-VAR assimilation without SSMI data (panel b.) and 4D-VAR using SSMI data (panel c.).

Considering panel a. as the truth, one can first notice that 4D-VAR overestimates PWC in the atlantic zone. This points out to a weakness of the assimilating model unable to take into account all the condensation/evaporation processes involved in this situation. However, the introduction of SSMI data dramatically improves the quality of the PWC analysis, since the magnitude and the shape of the PWC field produced by 4D-VAR becomes then comparable to the operational one (panel a).

It is also interesting to see (Fig. 16) the impact of these data on the wind field (here at the jet level) in a strong and quickly developing system. The area of Eastern Atlantic has been chosen since it corresponds to the situation described in section 2 36 hours before the particular storm hit Brittany and England. Panel (a) represents the 250 hPa wind field produced by 4D-VAR using SSMI, and panel (b) the 250 hPa wind difference between 4D-VAR without SSMI and 4D-VAR using SSMI. One can notice a strong impact over France and England (2.5 m/s). The inclusion of SSMI data reduces the activity of the

a)

type de mesure	nombre d'info.	4DVAR000	NOSSMI999	SSMI999
SYNOP	14396	42935.473	13763.637	13655.477
AIREP	4458	14892.342	5782.172	5690.204
DRIBU	455	1187.988	210.594	213.990
TEMP	44950	148088.237	60864.553	60081.587
PILOT	3998	9260.844	5225.212	5182.745

Tableau VI-1-a : Variation de la fonction coût Jo pour l'hémisphère Nord.

b)

type de mesure	nombre d'info.	4DVAR000	NOSSMI999	SSMI999
SYNOP	4530	8687.426	4560.056	4543.890
AIREP	588	1282.152	649.748	638.869
DRIBU	79	95.211	46.455	47.349
TEMP	4559	14297.869	6086.163	5978.644
PILOT	1892	5239.271	2234.347	2183.387

Tableau VI-1-b : Variation de la fonction coût Jo pour les tropiques.

c)

type de mesure	nombre d'info.	4DVAR000	NOSSMI999	SSMI999
SYNOP	1759	20225.878	2307.255	2292.435
AIREP	214	866.880	477.794	474.142
DRIBU	782	3797.975	1175.147	1112.667
TEMP	2772	17494.940	4632.473	4516.914
PILOT	2716	8881.088	3998.493	3905.630

Tableau VI-1-c Variation de la fonction coût Jo pour l'hémisphère Sud.

d)

type de mesure	nombre d'info.	4DVAR000	NOSSMI999	SSMI999
METEOSAT	3212	4088.385	1495.669	1476.250
GOES W	1364	1775.117	977.007	953.721
NOAA11 mer	9807	6682.316	5384.264	5322.198
NOAA11 terres	3036	1233.438	884.933	872.013
SSM/I	26658	27765.759	-	14185.531

Tableau VI-2 Variation de la fonction coût Jo pour les observations satellitales.

Fig 14 Contribution of the observational cost function for different observation types and geographical areas.
Panel (a): Northern hemisphere, conventional observations.
Panel (b): Tropics, conventional observations.
Panel (c): Southern hemisphere, conventional observations.
Panel (d): Globe, satellite derived observations.

First column: Observation type (a,b,c) or satellite (d).
Second column: Number of observations.
Third column: Initial value of the cost function.
Fourth column: Final value of the cost function (no SSMI in 4D-VAR).
Fifth column: Final value of the cost function (SSMI used in 4D-VAR).

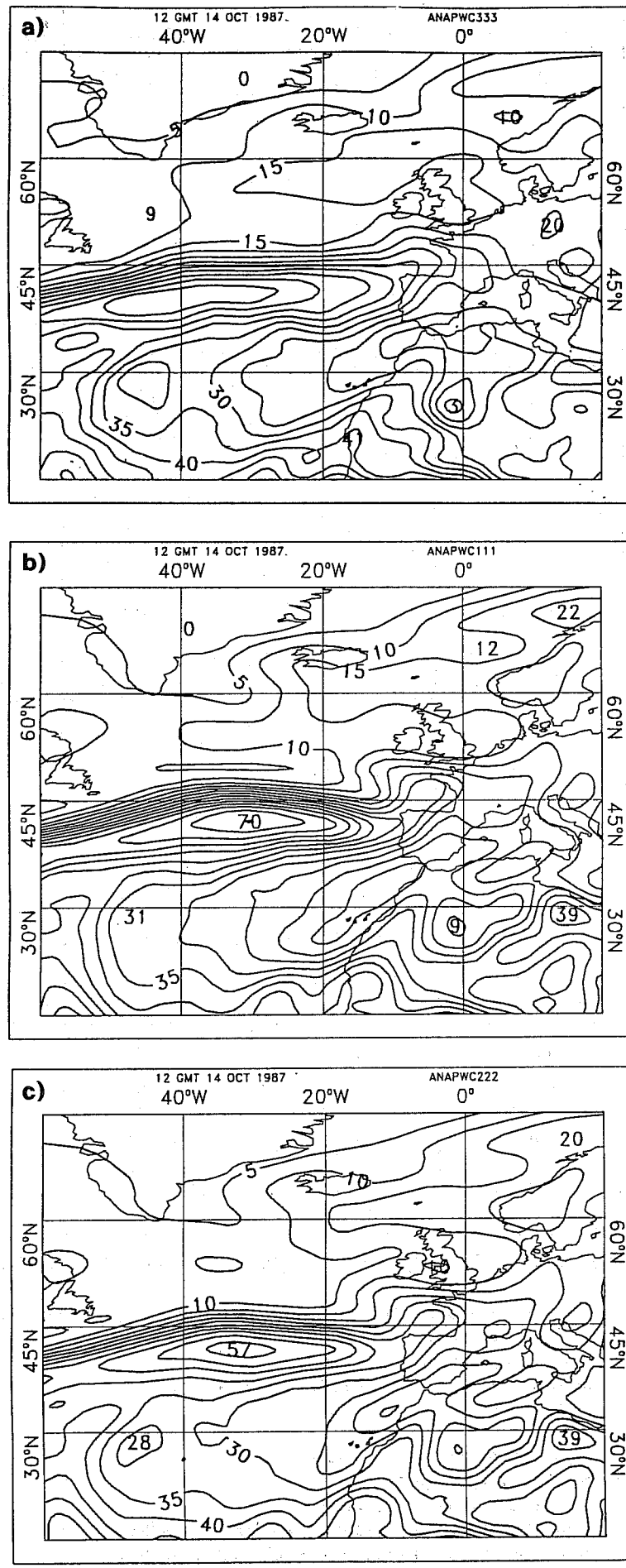

Fig 15 PWC analysed field from ECMWF operational analysis (panel a), 4D-VAR without SSMI (panel b) and 4D-VAR with SSMI (panel c). Unit: g/kg

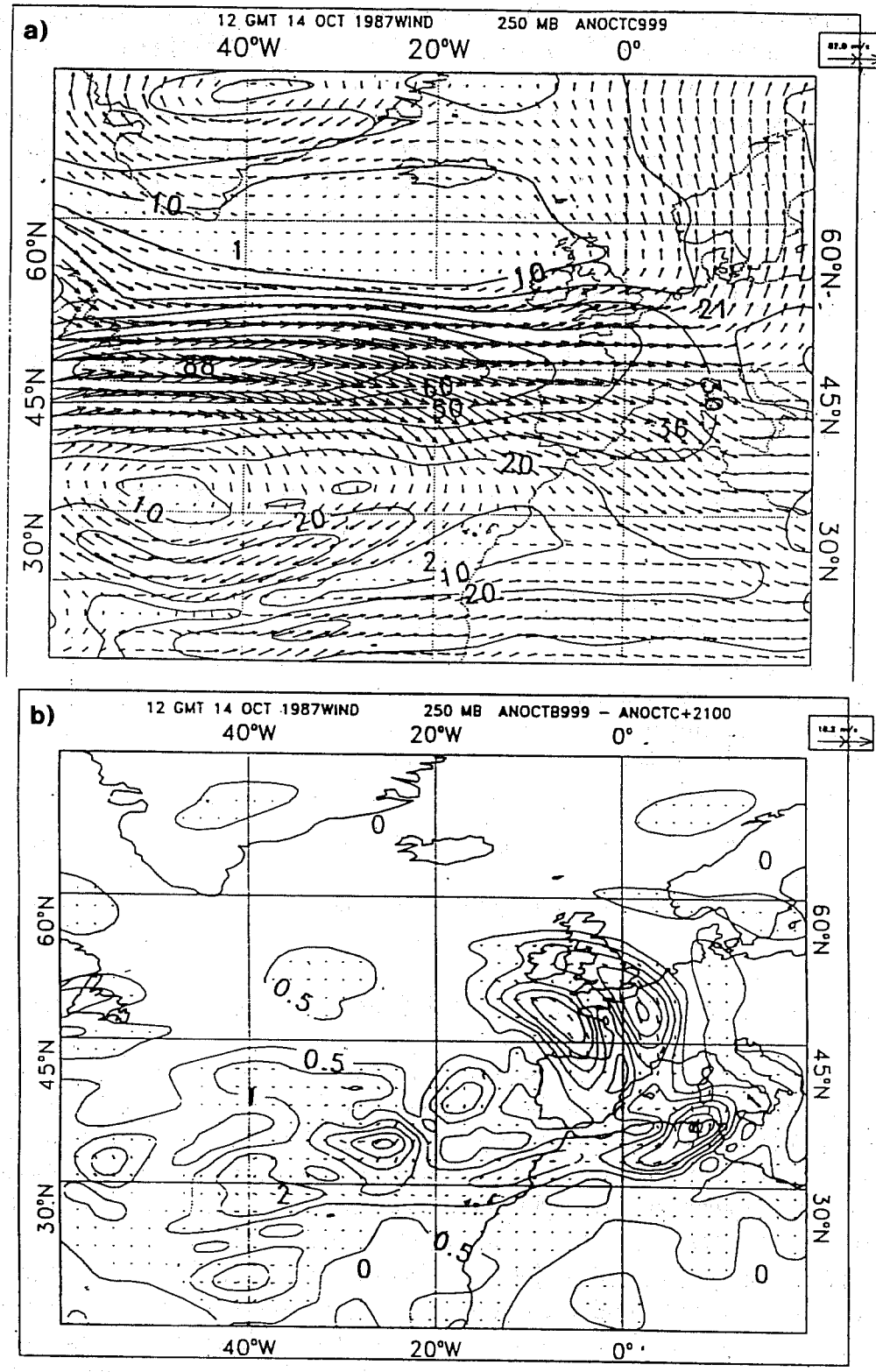

Fig 16 250 hPa analysed field from 4D-VAR with SSMI (panel a).
250 hPa wind difference between 4D-VAR without SSMI and 4D-VAR with SSMI (panel b).

system over England in the diffluent zone of the jet, which is compatible with the shape of the PWC field (Fig. 15).

An example of the impact of SSMI data on the wind field in the tropics is given in Fig. 17 which represents the difference between 4D-VAR with SSMI and 4D-VAR without SSMI, both for the PWC field (panel a) and for the 500 hPa wind field (panel b). One can see that the biggest wind increment over the selected area (panel b) reaches 3 m/s and corresponds to an area of strong PWC gradient. The same argument as in section 5 can be applied here. In our context PWC behaves as a passive tracer. In 4D-VAR, the observation of this tracer gives information on the advective part of the wind.

7 Concluding remarks.

This paper intended to review the kind of experiments which have been performed at ECMWF aiming at assimilating different types of satellite data in the 4D-VAR system. For all the trials experimented before, the first encouraging result is that 4D-VAR copes nicely with the introduction of asynoptic high-frequency data without degrading the fit to other conventional observations. Moreover, these observations are naturally used at the appropriate time, and are dynamically consistent with the atmospheric model solution (see section 6).4D-VAR can then takes benefit from a high density data coverage, which makes it a good candidate for assimilating future remotely-sensed data.

We have also seen that 4D-VAR implicitly uses flow-dependent structure functions and was then able to transfer accordingly in the vertical information coming from a surface observation (see sections 2 and 4).

Another strong point in favour of 4D-VAR is its intrinsic ability to infer information on non-directly observed components of the flow (see sections 3 and 6. This can be of vital importance for the improvement of the wind analyses in the tropics for instance.

Several issues however remain to be assessed before thinking of an operational implementation of 4D-VAR.

Firstly, the cost of the method remains a main issue. At the moment, a 24 hour 4D-VAR assimilation is equivalent to a 100 day forecast at least. We then have to find a way of cutting this cost down.

Secondly, the problem of having a realistic description of the physical processes is a general problem in 4D-VAR. Rabier et al. (1992) have shown that a realistic humidity analysis is impossible without condensation processes in the assimilating model. This seems mandatory for seeing a beneficial impact of assimilating humidity related observations such as SSMI data or TOVS humidity channels. One solution to the general problem is to develop the adjoint of all physical parameterizations. In that case, we might expect problems of convergence due to highly nonlinear processes in the assimilating model.

These two problems led us to the development of the so-called "4D-VAR in terms of increments" which is described in detail in Courtier et al. (1993). This method consists in approximating the full nondifferentiable minimization problem by a quadratic problem. The atmospheric state is still transported in time with the full model, but the minimisation is performed on the increments at a lower resolution and with a simplified model. While

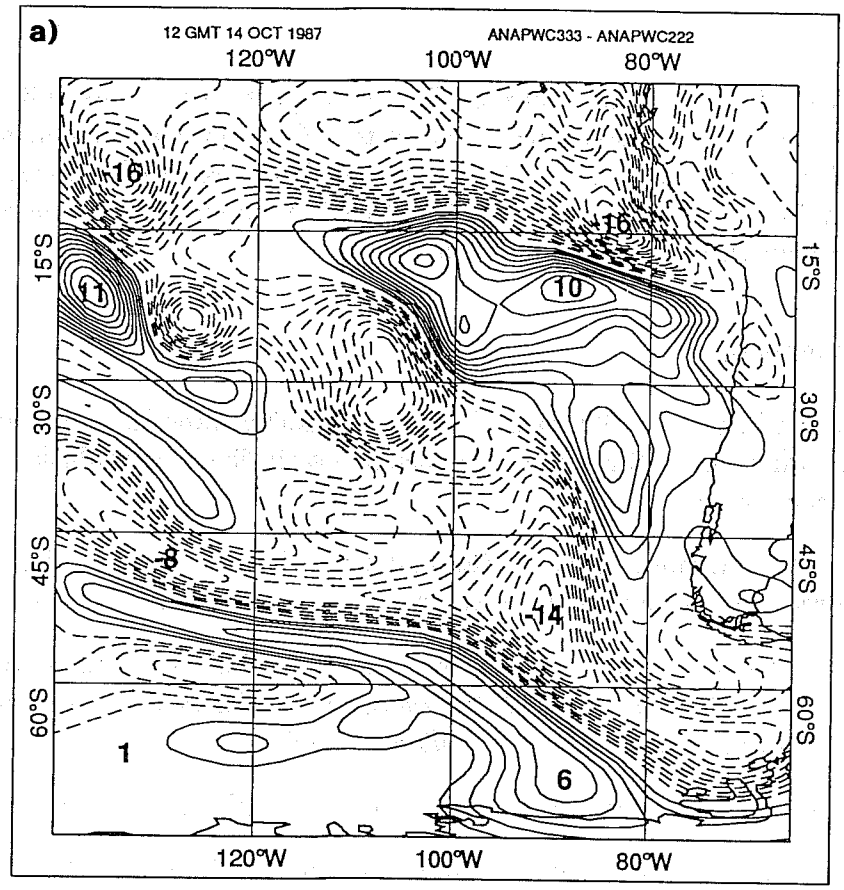

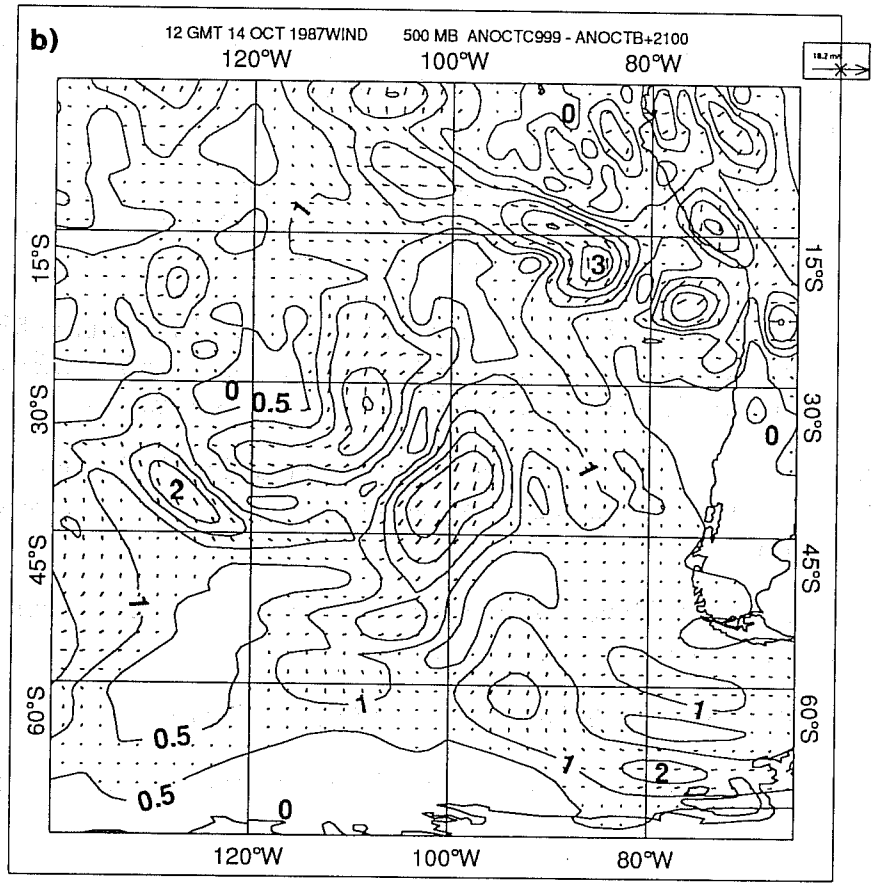

Fig 17 Panel a: PWC difference between 4D-VAR with SSMI and 4D-VAR without SSMI.
Panel b: 500 hPa difference between 4D-VAR with SSMI and 4D-VAR without SSMI.

cutting in this way the cost of the minimisation, we hope to get the benefit of having a full physics package to evolve the atmospheric state. This approach has been developed at ECMWF and is being tested in a 4D-VAR as well as in 3D-VAR context. The first results look promising and it is envisaged that the first operational implementation of 3D-VAR will be done in its incremental formulation.

8 References.

Andersson, E., J. Pailleux, J.-N. Thépaut, J. Eyre, A. McNally and P. Courtier, 1993: Use of cloud-cleared radiances in three/four-dimensional variational assimilation. *to appear in Q. J. R. Meteorol. Soc.*

Courtier, P. and O. Talagrand, 1990: Variational assimilation of meteorological observations with the direct and adjoint shallow-water equations. *Tellus*, **42A**, 531-549.

Courtier, P., J.-N. Thépaut and A. Hollingsworth, 1992: A strategy for operational implementation of 4D-VAR. *Proc. of ECMWF workshop on Variational Assimilation with Emphasis on Three-Dimensional Aspects. Volume II*, 437-462.

Daley, R., 1991: *Atmospheric Data Analysis*, Cambridge University Press.

Eyre, J.R., G.A. Kelly, A.P. McNally, E. Andersson and A. Persson, 1993: Assimilation of TOVS radiance information through one-dimensional variational analysis. *To appear in Q. J.R. Meteorol. Soc.*

Filiberti, M.-A., 1993: Assimilation dans des modèles météorologiques de données de vapeur d'eau intégrée mesurées par radiométrie hyperfréquence spatiale. *Thèse de doctorat de l'université de Paris VI.*

Francis, R., G. Graf, P. G. Edwards, M. McCaig, C. McCarthy, P. Dubock, A. Lefebvre., B. Pieper, P.-Y. Pouvreau, R. Wall, F. Wechsler, J. Louet and R. Zobl, 1991: The ERS-1 spacecraft and its payload. *ESA bulletin*, **65**, 27-48. ERS-1 Special Issue.

Heckley, W., P. Courtier, J. Pailleux and E. Andersson, 1992: On the use of background information in the variational analysis at ECMWF. *Proc. of ECMWF workshop on Variational Assimilation with Emphasis on Three-Dimensional Aspects.*, 49-93.

Hoffman, R. N., 1993: A preliminary study of the impact of the ERS1 *C*-band scatterometer wind data on the ECMWF global data assimilation system. *Journal of Geophysical Research*, **98**. In press.

Jarraud, M., J. Goas and C. Deyts, 1989: Prediction of an exceptional storm over France and Southern England. *Wea. For.*, **4**, 517-536.

Jazwinski, A. H., 1970: *Stochastic Processes and Filtering Theory.* Academic, New York.

Jones, W. L., L. C. Schroeder, D. H. Boggs, E. M. Bracalente, R. A. Brown, G. J.

Dome, W. J. Pierson, and F. J. Wentz., 1982: The SEASAT-A Satellite Scatterometer: The geophysical evaluation of remotely sensed wind vectors over the ocean. *Journal of Geophysical Research*, **87(C5)**, 3297–3317.

Lacarra, J. F., and O. Talagrand, 1988: Short-range evolution of small perturbations in a barotropic model. *Tellus*, **40A**, 81-95.

Long, A. E., 1991: Summary of CMOD2, Wismann, CMOD2-W and CMOD2-1 models. Document Number ESTEC/WMA/AEL/9101, Revision 1, ESTEC, European Space Agency.

Lorenc, A.C., 1986: Analysis methods for numerical weather prediction. *Q. J. R. Meteorol. Soc.*, **112**, 1177-1194.

Pailleux, J., W. Heckley, D. Vasiljevic, J.-N. Thépaut, F. Rabier, C. Cardinali, and E. Andersson, 1991: Development of a variational assimilation system. Technical Memorandum 179, ECMWF, Reading, U.K.

Price, J. C., 1976: The nature of multiple solutions for surface wind speed over the oceans from scatterometer measurements. *Remote Sensing Environ.*, **5**, 47-54.

Rabier, F. and P. Courtier, 1992: Four-dimensional assimilation in the presence of baroclinic instability. *Q. J. R. Meteorol. Soc.*, **118**, 649-672.

Rabier, F., P. Courtier, J. Pailleux, O. Talagrand, J.-N. Thépaut and D. Vasiljevic, 1992: Comparison of four-dimensional variational assimilation with simplified sequential estimation. *Proc. of ECMWF workshop on Variational Assimilation with Emphasis on Three-Dimensional Aspects.*, 271-325.

Schroeder, L. C., D. H. Boggs, G. Dome, I. M. Halberstam, W. L. Jones, W. J. Pierson, and F. J. Wentz, 1982: The relationship between wind vector and normalized radar cross section used to derive SEASAT-A satellite scatterometer winds. *Journal of Geophysical Research*, **87(C5)**, 3318–3336.

Schultz., H., 1990: A circular median filter approach for resolving directional ambiguities in wind fields retrieved from spaceborne scatterometer data. *Journal of Geophysical Research*, **95(C4)**, 5291–5304. Errata in number **C6**, page 9783.

Shaw D., P. Lonnberg, A. Hollingsworth and P. Unden, 1987: Data assimilation: The 1984/85 revisions of the ECMWF mass and wind analysis.*Q. J. R. Meteorol. Soc.*, **113**, 533-566.

Stoffelen, A. and D. L. T. Anderson, 1992a: ERS-1 scatterometer calibration and validation activities at ECMWF: A. The quality and characteristics of the radar backscatter measurements. In *European "International Space Year" Conference.*, Munich, Germany, 30 March - 5 April.

Stoffelen, A. and D. L. T. Anderson, 1992b: ERS-1 scatterometer data characteristics and wind retrieval skill. In *First ERS-1 Workshop*, Cannes, France, 4 - 6 November. To be published by European Space Agency.

Talagrand, O., 1988: Four-Dimensional Variational Assimilation. *Proc. of ECMWF seminar on Data assimilation and the use of satellite data.*, vol II 1-30.

Thépaut J.-N., and P. Courtier, 1991: Four-dimensional variational data assimilation using the adjoint of a multilevel primitive-equation model. *Q. J. R. Meteorol. Soc.*, **117**, 1225-1254.

Thépaut J.-N., 1992: Application des méthodes variationnelles pour l'assimilation quadri-dimensionnelle des observations météorologiques. *Thèse de doctorat de l'université Paris VI.*

Thépaut J.-N., D. Vasiljevic, P. Courtier and J. Pailleux, 1993a: Variational assimilation of conventional meteorological observations with a multilevel primitive equation model. *Q. J. R. Meteorol. Soc.*, **119**, 153-186.

Thépaut J.-N., R. N. Hoffman and P. Courtier, 1993b: Interactions of dynamics and observations in a four-dimensional variational assimilation. *Mon. Wea. Rev.*, **121-12**, 3393-3414.

Undén., P., 1989: Tropical data assimilation and analysis of divergence. *Mon. Wea. Rev.*, **117**, 2495-2517.

Vasiljevic, D., C. Cardinali and P. Unden, 1992: ECMWF 3D variational data assimilation of conventional observations. *Proc. of ECMWF workshop on Variational Assimilation with Emphasis on Three-Dimensional Aspects.*, 389-436.